

# A Novel Fusion of Optical and Radar Satellite Data for Crop Phenology Estimation using Machine Learning and Cloud Computing

Shahab Aldin Shojaezadeh<sup>1\*</sup>, Abdelrazek Elnashar<sup>1,2</sup>, Tobias Karl David Weber<sup>1</sup>

1 Section of Soil Science, Faculty of Organic Agricultural Sciences, University of Kassel, Witzenhausen 37213, Germany

2 Department of Natural Resources, Faculty of African Postgraduate Studies, Cairo University, Giza 12613, Egypt

\*Corresponding Author: [shahab@uni-kassel.de](mailto:shahab@uni-kassel.de)

## Abstract

Crop phenology determines crop growth stages and is valuable information for decision makers to plant and adapt agricultural management strategies to enhance food security. In the era of big Earth observation data ubiquity, attempts have been made to accurately predict crop phenology based on Remote Sensing (RS) data. However, most studies either focused on large scale interpretations of phenology or developed methods which are not adequate to help crop modeler communities on leveraging the value of RS data evaluated using more accurate and confident methods. Here, we estimate phenological developments for eight major crops and 13 phenological stages across Germany at 30m scale using a novel framework which fuses Landsat and Sentinel 2 (Harmonized Landsat and Sentinel data base; HLS) and radar of Sentinel 1 with a Machine Learning (ML) model. We proposed a thorough feature fusion analysis to find the best combinations of RS data on detecting phenological developments based on the national phenology network of Germany (German Meteorological Service; DWD) between 2017 and 2021. The nation-wide predicted crop phenology at 30 m resolution showed a very high precision of  $R^2 > 0.9$  and a very low Mean Absolute Error (MAE)  $< 2$  (days). These results indicate that our fusing strategy of optical and radar datasets is highly performant with an accuracy highly relevant for practical applications, too. The subsequent uncertainty analysis indicated that fusing optical and radar data increases the reliability of the RS predicted crop growth stages. These improvements are expected to be useful for crop model calibrations and evaluations, facilitate informed agricultural decisions, and contribute to sustainable food production to address the increasing global food demand.

**Keywords:** Crop monitoring, Agriculture, Remote sensing, HLS, Uncertainty analysis, Germany

## 1. Introduction

The phenological development stages determine the onset and duration of plant growth events. Knowledge on these phenological stages plays a crucial role in agricultural practices to guide decision makers on planning irrigation schedules and fertilization strategies ([Meroni et al. 2021](#)). It is also important for monitoring plant productivity, plant health, and identify the incidence of pests and diseases ([Schwartz 2003](#); [Xia et al. 2015](#)). Phenological patterns in natural landscapes could also serve as an indicators of biodiversity ([Viña et al. 2016](#)) that enables the evaluation of the impact of climate change ([Badeck et al. 2004](#)) and land-use alterations on ecosystems ([Morellato et al. 2016](#)). Thus, applications for accurate and precise estimations of phenological development over large scales at high spatial resolution exists, yet the efforts to gauge crop phenological stages accurately are still an ongoing challenge from field to large scale.

Crop phenology is typically assessed by restricted labor intensive in situ field observations usually limited to point locations in specific regions. To overcome the resulting data scarcity, researchers have proposed various methods to estimate crop phenological events at large spatial scales based on climate data ([Gerstmann et al. 2016](#); [Li et al. 2021](#)), carbon and nitrogen cycles ([Holzworth et al. 2014](#); [Peano et al. 2021](#)), and Earth Observation (EO) data ([Babcock et al. 2021](#); [Tian et al. 2021](#); [Vijaywargiya and Nidamanuri 2023](#)). EO data, particularly multispectral imagery such as Landsat and Sentinel-2 satellites, has been used to estimate phenology at regional to global scales ([Katal et al. 2022](#); [Tran et al. 2023](#); [Yang et al. 2023a](#)). Recently, Synthetic Aperture Radar (SAR) data is gaining attention because of its weather resilience ([Li et al. 2023](#); [Wang et al. 2019](#); [Zhao et al. 2022](#)). While SAR data has been shown to provide valuable information about phenological developments ([Lobert et al. 2023](#)), this is still under debate ([Mercier et al. 2020](#); [Meroni et al. 2021](#)); underlining the need for further exploration. In addition, [Lobert et al. \(2023\)](#) showed that SAR and multispectral data fusion is ideal to estimate phenological development. Although EO-based studies on estimating phenological developments mostly rely on Vegetation Indices (VIs), other EO based parameters such as surface soil temperature ([Stone et al. 1999](#); [Yuan et al. 2022](#)) and surface soil moisture ([Liu et al. 2022b](#); [Stöckli and Vidale 2004](#)), which have long history in phenological studies, could be beneficial to estimate phenological stages. Hence, fusing optical and SAR imageries along with prior knowledge about affective parameters (e.g., surface soil temperature) on plant growth could bridge the gap between field, experimental studies, and EO data.

Various methods using EO data have been developed to estimate phenological development and stages. These include analyzing time series of VIs, well-known as Land Surface Phenology (LSP, ([Babcock et al. 2021](#); [Nietupski et al. 2021](#); [Tran et al. 2023](#); [Yang et al. 2023a](#))), combining VIs and/or satellite spectrums (i.e., raw data) with Physical Crop Models (PCM, ([MacBean et al. 2015](#); [Viswanathan et al. 2022](#); [Worrall et al. 2023](#))), Machine Learning algorithms (ML, ([Katal et al. 2022](#); [Li et al. 2021](#); [Lobert et al. 2023](#); [Ma et al. 2023](#); [Zhou et al. 2021](#))), and phenology matching models such as shape model fitting (SMF, ([Diao et al. 2021](#); [Liu et al. 2022a](#))) at various regional to global scales ([Tran et al. 2023](#)). LSP is a well-known method that focusses on overall crop growth stages to estimate phenological events at the start (SoS) and end (EoS) of the growing season; for extensive discussion please refer to [Zeng et al. \(2020\)](#). While, recent studies focused on methods that explicitly estimate predefined phenological stages coinciding with ground observations ([Canisius et al. 2018](#); [Diao et al. 2021](#); [Liu et al. 2022a](#); [Lobert et al. 2023](#); [Wang et al. 2019](#)), there is still a need to enhance the proposed methods based on EO-data. With today's richness of EO data and advancements in ML models, there is a lot of hope to synergize ML-EO-based model imputed with ground observations to improve the accuracy to estimate phenological developments of crops ([Kooistra et al. 2023](#)). Although various studies explored the potential of ML models to predict phenology ([Czernecki et al. 2018](#); [Wang et al. 2023](#); [Worrall et al. 2023](#); [Xin et al. 2020](#); [Yang et al. 2023b](#)), these studies are often limited to specific crops or phenological stages, limiting their applicability to a broader range of agricultural scenarios ([Lobert et al. 2023](#); [Tedesco et al. 2021](#)).

Therefore, this study aims to estimate phenology, fusing Landsat, Sentinel-1, and Sentinel-2 satellite imagery to derive various vegetation indices, including Plant Phenological Index (PPI), Radar Vegetation Index (RVI), and soil parameters of Surface Soil Moisture (SSM), and Surface Temperature (ST) inputs, with Digital Elevation Model (DEM) data as input features for a Tree-based gradient boosting ML algorithm of LightGBM. As ground truth, the database of the German Weather Service on phenological observation was utilized as a reference for phenological stages, which covers all of Germany. The study focused on eight major crops – maize, spring and winter barley, spring oat, sugar beet, winter rapeseed, winter rye, and winter wheat – and encompassed 13 phenological stages over the period 2017 to 2021. Approximately 150,000 phenology observations from ground stations were compared with data from nearby fields to create a

regression model for estimating phenological stages based on EO data. This study is trying to answer the following questions:

- 1- How can the fusion of EO data enhance the estimation of phenological stages, and how does each satellite contribute to this estimation?
- 2- What is the value of incorporating soil states along with VIs from satellites in phenology estimation?
- 3- How effectively can EO data represent the spatio-temporal variations of phenological events at DWD stations in Germany?

## **2. Materials and methods**

### **2.1. The study area and reference data**

The comprehensive phenology database of the German Meteorological Service (DWD) was used as reference data. This database is well-known for its long-term volunteered-based observations (~1200 trained observers) that started in 1950 with over 10 million observations and 1000 stations across Germany ([Kaspar et al. 2015](#)). The DWD phenology database includes phenological stages for various plants. Maize (corn; *Zea mays L.*), spring and winter barley (*Hordeum vulgare L.*), spring oat (*Avena sativa L.*), sugar beet (*Beta vulgaris L.*), winter rapeseed (*Brassica napus L.*), winter rye (*Secale cereale L.*), and winter wheat (*Triticum aestivum L.*) were selected among others that had consistent observations through time. Our choice led to 862 stations across Germany that included more than 150,000 observations for thirteen specific phenological stages between 2017 and 2021. The study area and DWD stations are shown in Fig. 1A.

The DWD has an explicit definition for phenology stages; however, Phenological Development Stages of Plants (BBCH) standard was used in this study for the larger scientific community and operational goals ([Kaspar et al. 2015](#)). The phenological stages that are available include seeding (BBCH~0), emergence (~10), rosette formation (~14), growth in height or shooting (~31), closed stand (~35), bud formation, heading or tassel emergence (~51), the tip of tassel visible (~53), the beginning of flowering (~61), general flowering (~65), mil ripeness (~75), wax-ripe stage (~83), full or yellow ripeness (~87), and harvest (~89). For the harvest stage, the exact BBCH scale is not available, but we selected BBCH equal to 89 before starting the latest phase of the plant (beginning of dormancy or Senescence~90). Each record in the database holds a quality flag that we used to



filter doubtful observations. A specific routine was also used to remove spatial outliers and extract crop field boundaries in each DWD station.

## **2.2. Crop field boundaries**

In previous studies, various radiuses were proposed to identify a representative observation radius from 1 km to 20 km around the DWD stations ([Kowalski et al. 2020](#); [Lobert et al. 2023](#); [Tian et al. 2021](#)). Following the DWD suggestions, we fixed the observation radius to 2 km, which is commonly used ([Kaspar et al. 2015](#); [Lobert et al. 2023](#)). A Crop Type Map (CTM) of Germany ([Blickensdörfer et al. 2022](#)) was used to identify the crop type in the 2x2-km rectangle around DWD stations (Figs. 1B-D). For each identified crop field, we followed a two-step approach to remove boundary affects (from e.g. hedge rows, or field boarders, headlands, ...) by removing a 30 m inside buffer in the field followed by an outside buffer of 10 m. Finally, each field larger than 2 hectares area was selected as a candidate field as suggested by [Lobert et al. \(2023\)](#)

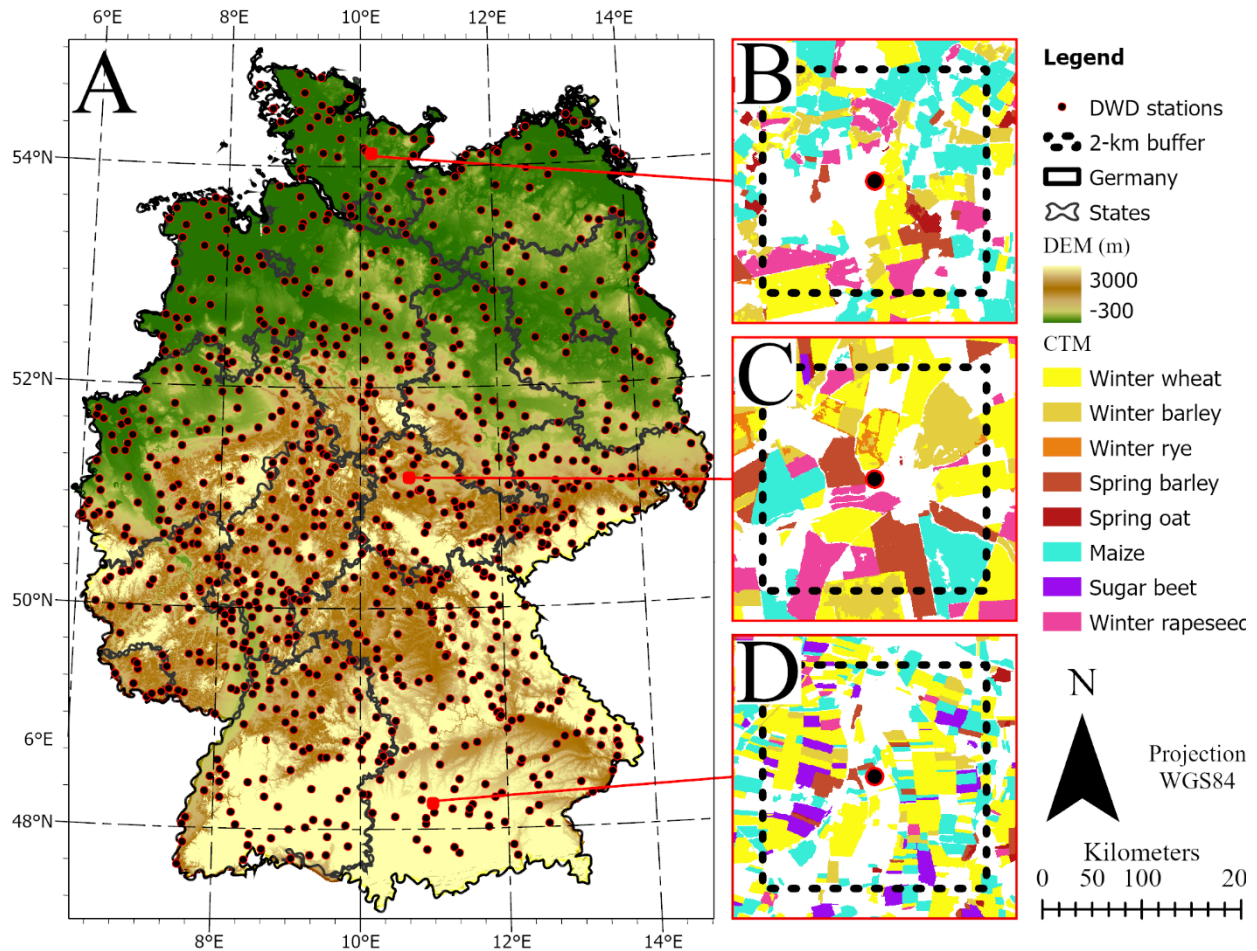


**Figure 1** Study area and distribution of DWD stations (A) with 2-km buffer boundaries at selected stations (B-D) with digital elevation model (DEM) crop type map (CTM).

## 2.3. Remote sensing data and indices

### 2.3.1. Sentinel-1

Sentinel-1 (S1) mission is a constellation of two polar-orbiting satellites that carry a C-band synthetic aperture radar (SAR) instrument. The primary advantage of this satellite is the acquisition of imagery regardless of the weather conditions which makes it ideal for land monitoring. However, topography can affect both the position of the pixel (known as geometric distortions of Earth's surface) and the brightness of radar return (Small 2011). Therefore, we used the Radiometrically Terrain Corrected (RTC) products of Microsoft Planetary Computer (MPC, Source et al. (2022)) utilizing Spatio-Temporal Asset Catalogs (STAC) in Python (Section 2.8). The Radar Vegetation Index (RVI) is a well-known index for monitoring vegetation dynamics

(Mandal et al. 2020). It has a meaningful correlation with the Leaf Area Index (LAI) (Pipia et al. 2019) and calculated using the following Eq. (1):

$$RVI = \frac{4VH}{VH + VV} \quad (1)$$

Where  $VH$  is vertical transmit and horizontal receive polarization, and  $VV$  is vertical transmit and vertical receive polarization. Previous studies showed that  $RVI$  is an excellent alternative for optical vegetation indices at cloudy pixels (Villarroya-Carpio et al. 2022). However, it is affected by surface soil moisture (Khabbazan et al. 2022; Szigarski et al. 2018). Therefore, we used an approach to consider the effect of soil moisture on  $RVI$  by calculating surface soil moisture ( $SSM$ ; in %) from Sentinel-1 satellite using Bauer-Marschallinger et al. (2019) proposed method as follow:

$$SSM = \frac{VV - \sigma_{dry}}{\sigma_{wet} - \sigma_{dry}} \quad (2.1)$$

$$\sigma_{dry} = \frac{0 - d}{k} \quad (2.2)$$

$$\sigma_{wet} = \frac{100 - d}{k} \quad (2.3)$$

$$k = \frac{90 - 10}{\sigma_{90} - \sigma_{10}} \quad (2.4)$$

$$d = 90 - k\sigma_{90} \quad (2.5)$$

$$\sigma_{10}, \sigma_{90} = VV_{quantile\ 10\%}^{time}, VV_{quantile\ 90\%}^{time} \quad (2.6)$$

Where  $\sigma_{10}, \sigma_{90}$  are 10 and 90 percentiles of  $VV$ ,  $k$  and  $d$  [all in dB] are scale factors to extract dry ( $\sigma_{dry}$ ; dB) and wet ( $\sigma_{wet}$ ; dB) conditions. This method has several limitations such as sensitivity to canopy height and density (Zeyliger et al. 2022). However, it provides valuable information about surface soil moisture variability to combine the effect of soil moisture on monitoring canopy dynamics. The  $\sigma_{dry}$  and  $\sigma_{wet}$  were estimated for the long term (2015–2022) to better reflect the effect of dry and wet pixels.

### 2.3.2. Harmonized Landsat and Sentinel-2 (HLS)

The HLS dataset is shaped by harmonizing the Operational Land Imager (OLI) sensor onboard the Landsat-8 and -9 satellites, and the Sentinel-2 Multi-Spectral Instrument (MSI) that onboard two satellites of Sentinel-2A and -2B ([Claverie et al. 2018](#)). The HLS dataset provides high-quality products that use consistent methods for atmospheric correction, Bidirectional Reflectance Distribution Function (BRDF) correction, and spectral band adjustment for both OLI and MSI.

We used the HLS dataset to calculate the Plant Phenological Index (*PPI*;  $m^2 m^{-2}$ ) which is a physically based index for monitoring plant phenology from optical images ([Jin and Eklundh 2014](#)). This index is calculated based on the radiative transfer equation as follows:

$$PPI = -K \ln \left( \frac{MDVI - DVI}{MDVI - SDVI} \right) \quad (3.1)$$

$$DVI = NIR - red \quad (3.2)$$

$$K = \frac{1}{4[d_c + 0.5(1 - d_c)/\cos \theta_{SZA}]} \frac{1 + MDVI}{1 - MDVI} \quad (3.3)$$

$$d_c = 0.0336 + 0.0477/\cos \theta_{SZA} \quad (3.4)$$

Where  $d_c$  [unitless] is an instantaneous diffuse fraction of solar radiation at sun zenith angle  $\theta_{SZA}$ , *NIR* and *red* are satellite reflectance bands, *MDVI* is the maximum *DVI* [unitless], *K* is a gain factor [unitless], and *SDVI* is the *DVI* of the soil (=0.09; unitless) ([Jin and Eklundh 2014](#)). The *PPI* was calculated using HLS products in NASA's Common Metadata Repository (CMR) platform with the STAC package in Python.

The *PPI* is insensitive to the influence of snow (at high northern latitudes), noises of satellite imageries during seasonal transitions, and saturation in the middle of the season in contrast to the Normalized Difference Vegetation Index (NDVI) and Enhanced Vegetation Index (EVI) ([Jin and Eklundh 2014](#); [Tian et al. 2021](#)). The *PPI* has a strong linear relationship with LAI ([Jin and Eklundh 2014](#)). However, the soil brightness effect is moderate on *PPI* at the start of the season at lower LAI, with decreasing levels when LAI rises ([Jin and Eklundh 2014](#)). Previous studies indicated temperature plays a key role in plant growth stages, especially at the start of the season ([Hatfield and Prueger 2015](#)). Therefore, we used surface soil temperature (SST, °C) to better identify the

bare soil and vegetated pixels from temperature variations, when PPI is affected by soil brightness which could be considered a novel point in this study.

#### **2.4. Elevation data**

After the Copernicus Digital Elevation Model (CDEM) was released in 2019, the most recent DEM dataset in 30 m resolution, various studies investigated the accuracy of this dataset ([Guth and Geoffroy 2021](#); [Li et al. 2022a](#); [Liu et al. 2023](#)). There is wide consensus that this dataset is a very reliable dataset. However, like any DEM dataset, it is also affected by trees and buildings. In solution, [Hawker et al. \(2022\)](#) used a Machine Learning (ML) model to remove buildings and tree height biases from CDEM named Forest And Buildings removed Copernicus DEM (FABDEM) to overcome this limitation. Some recent studies have evaluated the accuracy of FABDEM and approved that the accuracy in representing bare land terrains is of excellent reliability ([Dandabathula et al. 2023](#); [Marsh et al. 2023](#)). Since agroforestry is common in Germany, the FABDEM dataset allowed us to remove the effect of trees next to and in crop fields. It is a crucial factor in phenology estimation when the DEM dataset plays a role in model features. To be conservative about trees' effect on spatio-temporal estimation of phenology stages, we assessed the accuracy of CTM data by comparing it to the European Space Agency (ESA) World Cover ([Zanaga et al. 2021](#)) and Japan Aerospace Exploration Agency (JAXA) global forest/non-forest (FnF) ([Shimada et al. 2014](#)) for the year 2020. For eight selected crops, incorrectly classified crop field boundaries, and differences between FABDEM and CDEM were assessed in 862 DWD stations (Fig. S1). This idea approved that FABDEM as a DEM dataset should be used for spatial estimation of phenology stages.

Altitude is the major factor that changes the climate factors and consequently the plant growth, while slope and aspect affects the diversity and density of plants ([Marini et al. 2007](#); [Singh 2018](#)). Therefore, we used altitude and its derivatives of slope and aspect in this study. For slope and aspect calculation, the `xarray-spatial` package in Python was employed (see <https://github.com/makepath/xarray-spatial>).

#### **2.5. Preprocessing reference data and satellite data**

The HLS dataset provides temporal revisiting of 2–3 days, which is ideal for vegetation monitoring. However, due to frequent cloud cover in winter and fall in Germany, satellite images had to be masked (images with cloud <90% followed by masking cloud, cirrus, and cloud shadows

using image metadata). Therefore, optical and SAR parameters were composited to weekly median to remove cloud masking and bias effects. Furthermore, to take out undesired noises and artifacts, Savitzky–Golay filter were used for time series smoothing ([Savitzky and Golay 2002](#)). A window size of four by order of three was selected to conserve more information while suppressing noises based on mean squared error and structural similarity indices (Fig. S2). This method enabled us to preserve the peak values of optical and SAR parameters in growing seasons. The min-max normalization technique was used to normalize the optical and SAR parameters for each crop–year. This normalization rescaled features to standardized units and improved model training performance by preventing features with larger numeric ranges from distorting the scale and exposing more meaningful patterns while also accelerating gradient descent convergence of hyper tuning (Section 2.6). The preprocessed optical and SAR values were then resampled to daily resolution using linear interpolation to match the time stamps of DWD phenology reference data which could be considered another novel point in this study. The preprocessing algorithm of satellite data time series is described in Fig S3. A peer-to-peer analysis matched each phenology phase and crop type at DWD stations with the corresponding satellite data. As an example, Fig. 2 shows the preprocessed data for all crops at a sample DWD station in Empede town of Neustadt in Lower Saxony for 2018.

## 2.6. ML model

Tree-based gradient boosting (GB) learning algorithms recently got attention in many fields of science and they showed promising performances in remote sensing of vegetation and land use land cover classification ([Gao et al. 2023](#); [Zhang et al. 2021](#)). Due to the structure of the GB methods, they may deal with highly nonlinear interrelations between predictors and response variables in the form of an ensemble of weak predictions ([Chen and Guestrin 2016](#)). Various GB models are introduced and among them, we selected the novel LightGBM ensemble tree model with various features such as scalability, efficiency, and handling large-scale data ([Ke et al. 2017](#)). The LightGBM was executed in Python using the LightGBM package (see <https://github.com/microsoft/LightGBM>).

Although GB models are efficient, they are relatively problematic in finding the global optimum. Therefore, we employed the hyper-tuning algorithm of Optuna in Python to find the best parameters of the LightGBM model ([Akiba et al. 2019](#)). The Optuna is a hyperparameter

optimization framework that uses the advanced sampling technique of a Tree-structured Parzen Estimator (TPE) sampler. The TPE sampler can make a multivariate suggestion for parameters similar to advanced Bayesian Optimization and HyperBand (BOHB) algorithm ([Falkner et al. 2018](#)). It enabled us to use various parameters and a complex objective function to find the global optima of the LightGBM model parameters. For hyper tuning of LightGBM best parameters, this study focused on “n\_estimators”, “learning\_rate”, “objective”, “seed”, “early\_stopping\_round”, and “metric” parameters. Inspired by Optuna, we proposed an efficient objective function for hyper-tuning (Section 2.7). We restricted the model's predictions to a one-year period (365 days) during hyperparameter tuning. If the model's predicted day of the year falls outside of the one-year period, the trial is considered unsuccessful and assigned an infinite for loss function value. It helps Optuna to focus on rationally feasible solutions.



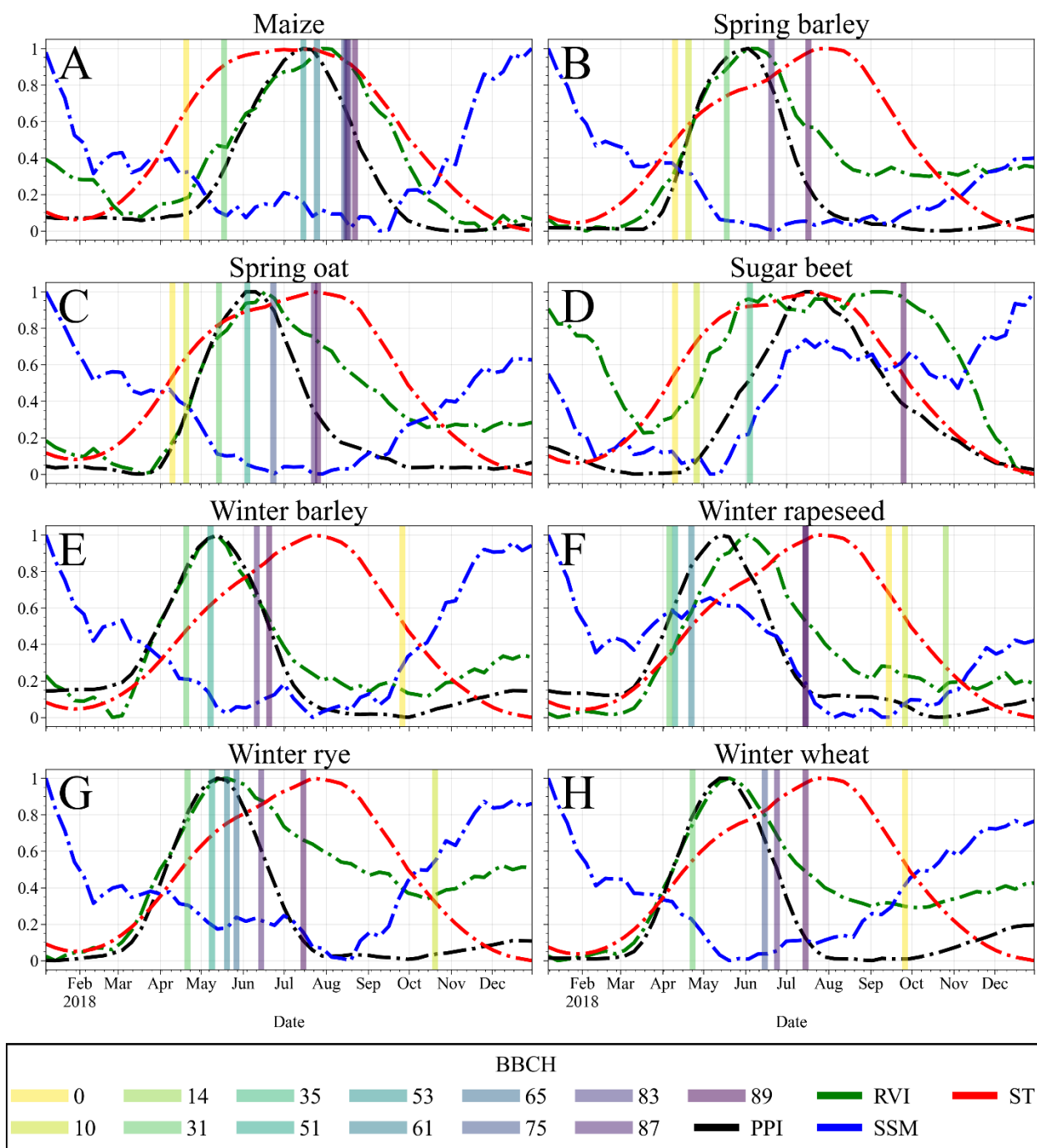


**Figure 2** Time series of estimated EO-based parameters for each crop at different BBCH stages in 2018. Note: BBCHs equal to 0, 10, 14, 31 for winter crops are for the next growing season (2019).

We used 60% of the data for training model, 20% for validation, and 20% for evaluation. A stratified and shuffled sampling method was operated on data splitting to ensure that each split had a representative distribution of crops and BBCH stages. During hyperparameter tuning, we trained

each model 100 times to find the best parameters. In each trial, we used ten k-fold stratified cross-validations with early stopping (between 5 and 20 epochs selected by Optuna) to prevent overfitting and ensure a global optimum. Additionally, to reduce the impact of randomness on the ML model, we used 30 different random seeds in hyperparameter tuning trials and repeated the modeling 10 times with different random seeds to initialize TPE sampler from different initial points. This approach supported our evaluation to create an ensemble prediction and let us perform uncertainty analysis. We employed an uncertainty toolbox package in Python to quantify uncertainty ([Chung et al. 2021](#)). Additionally, to better understand the predictive uncertainty of the models, we used conformal predictions to find the uncertainty intervals from almost zero to one standard deviation, using MAPIE package in python (<https://github.com/scikit-learn-contrib/MAPIE/tree/master>). MAPIE provided a probabilistic prediction method which is distribution-free and theoretically guaranteed to produce realistic forecasts ([Angelopoulos and Bates 2021](#)).

The effect of each predictor on the final estimation of the ML models was analyzed using the SHapley Additive exPlanations (SHAP) method. SHAP is an agnostic model that explains the effect of each parameter on the final output while a set of input samples is perturbed ([Lundberg and Lee 2017](#)). SHAP considers feature interactions and supplies a localized interpretation of feature importance, resulting in a more in-depth understanding of the significance of each feature for a specific instance. We employed the SHAP package in Python to estimate SHAP values for ML models (see <https://github.com/shap/shap>). The flowchart of this study is shown in Fig. 3.

The proposed framework for the estimation of phenology relies on the CTM, phenology stage (BBCH), geospatial location (latitude and longitude), year, DEM and its derivatives, and EO parameters (e.g., PPI) from optical and SAR satellite data (Fig. 2). These parameters were used to train, validate, and evaluate a regression ML model to extract the start date of each phenology stage. To help the ML model learn the temporal variability of crop growth efficiently, we assumed  $\pm 3$  days of exact phenology date is a good approximation to train ML model suggested by ([Lobert et al. 2023](#)). Thus, for the ML model, crop type information and phenology stages were used as a categorical predictor and other variables as a numerical predictor, while the day of year is the target variable. We proposed eleven feature sets that were evaluated for model evaluation in Table 1. We

also conducted a correlation analysis between target variable (day of year) and input features (Fig. S4), which shows each parameter we introduced has a strong correlation with target variable.

Furthermore, post-hoc tests ([Tamhane 2007](#)) and Multi Criteria Decision Making (MCDM) ([Ishizaka and Nemery 2013](#)) algorithms were used to identify the optimal feature set. Kolmogorov-Smirnov ([Massey Jr 1951](#)) and Shapiro-Wilk test ([Shapiro and Wilk 1965](#)) were used to test for normality. Depending on the results of normality tests, Tukey’s test ([Tukey 1949](#)) or Conover’s test ([Conover and Iman 1981](#)) were used for pairwise significant tests. For MCDM analysis, well-known algorithms of Technique for Order of Preference by Similarity to Ideal Solution (TOPSIS) ([Hwang et al. 1981](#)), and Preference Ranking Organization Method for Enrichment of Evaluation (PROMETHEE II) ([Brans et al. 1986](#)) were used to make accurate decisions between feature sets. For post-hoc analysis, the `scikit_posthocs` package in Python (see <https://github.com/maximtrp/scikit-posthocs>), and for MCDM analysis, comprehensive `pymcdm` package in Python (see <https://gitlab.com/shekhand/mcda#c4>) were used ([Kizielewicz et al. 2023](#)).

**Table 1 Full combinatory** feature sets for model evaluation to estimate crop phenology.

| <b>ID</b> | <b>Feature set *</b> | <b>Spatial resolution (m)</b> | <b>References</b>   |
|-----------|----------------------|-------------------------------|---|
| 1         | RVI                  | 10                            | ( <a href="#">Ma et al. 2023</a> ; <a href="#">Yang et al. 2021</a> ) |
| 2         | PPI                  | 30                            | ( <a href="#">Tian et al. 2021</a> )                                  |
| 3         | ST                   | 30                            | This study.   |
| 4         | RVI-SSM              | 10                            | This study.   |
| 5         | PPI-ST               | 30                            | This study.   |
| 6         | PPI-RVI              | 30                            | This study.   |
| 7         | RVI-ST               | 30                            | This study.   |
| 8         | PPI-SSM              | 30                            | This study.   |
| 9         | PPI-RVI-SSM          | 30                            | This study.   |
| 10        | PPI-RVI-ST           | 30                            | This study.   |
| 11        | PPI-RVI-SSM-ST       | 30                            | This study.   |

\* DEM and its derivatives are static input layers in this study.

## 2.7. Performance metrics

The ML model performance to predict phenology stages is evaluated by multiple metrics of the Nash-Sutcliffe Efficiency (NSE) ([Nash and Sutcliffe 1970](#)), Kling-Gupta Efficiency (KGE) ([Gupta et al. 2009](#)), Root Mean Squared Error (RMSE), Mean Bias Error (MBE), and Negative Log-Likelihood (NLL) as follows:

$$\begin{aligned}
 NSE &= 1 - \frac{\sum_{i=1}^n [y_i - \hat{y}_i]^2}{\sum_{i=1}^n [y_i - \bar{y}]^2} & ; & \quad -\infty < NSE \leq 1 \\
 KGE &= 1 - \sqrt{(c-1)^2 + \left(\frac{\sigma}{\hat{\sigma}} - 1\right)^2 + \left(\frac{\mu}{\hat{\mu}} - 1\right)^2} & ; & \quad -\infty < KGE \leq 1 \\
 RMSE &= \sqrt{\frac{\sum_{i=1}^n (y_i - \hat{y}_i)^2}{n}} & ; & \quad 0 \leq RMSE < +\infty \\
 MBE &= \frac{\sum_{i=1}^n y_i - \hat{y}_i}{n} & ; & \quad -\infty < MBE < +\infty \\
 NLL &= \frac{n}{2} \log(2\pi) + \frac{n}{2} \log(\sigma^2) + \frac{1}{2\sigma^2} \sum_{i=1}^n (y_i - \mu)^2 & ; & \quad -\infty \leq NLL \leq 0
 \end{aligned} \tag{5}$$

Where,  $y_i$  and  $\hat{y}_i$  are observed and estimated values of phenology date [day of year], respectively,  $\bar{y}$  is the average value of observation,  $c$  is the linear correlation between observed and estimated,  $\sigma$  is the standard deviation of observed and  $\hat{\sigma}$  is the standard deviation of estimated, and  $\mu$  is the observed average and  $\hat{\mu}$  is the estimated average, and  $n$  denotes the length of observation.

The NSE metric configures model performance to consider distances between estimation and observation values and patterns, while the KGE metric evaluates statistical differences between estimation and observation values and patterns. In contrast, the RMSE is a symmetric and simple metric that considers only the difference between estimation and observation with the root mean squared unit of the target variable. In addition, MBE is used to be sure that model is not systematically biased. Thus, we proposed an objective function based on these metrics in the form of  $[(1 - NSE) + (1 - KGE)] \times [RMSE + abs(MBE)]$  to be minimized. This objective function provides a ‘‘holistic view for Optuna’’ and was shown to shape objective function space favorably in searching for a global optimum, while ensuring matching units. We carefully analyzed the proposed loss function based on various parts (Fig. S5). Results convinced us that the proposed loss function is necessary to consider several metrics in a loss function rather than focusing in specific metrics for model calibration.

## 2.8. Processing environment

In this study, we used the most recent cloud based standardization to access satellite and big data sources named STAC package in Python (<https://github.com/stac-extensions/eo/>). This open standard for encoding and sharing RS data can be used to describe a wide variety of geospatial data sources, harnessing the capabilities of Python and free/commercial databases. Although in some cases to represent phenological maps, we used Google Earth Engine (GEE), most of the computations, analysis, preprocessing and postprocessing of the proposed framework has been established in STAC in terms of different reasons such as high performance cloud based computations, clustering and partitioning multiplications, and flexible access through various sources.

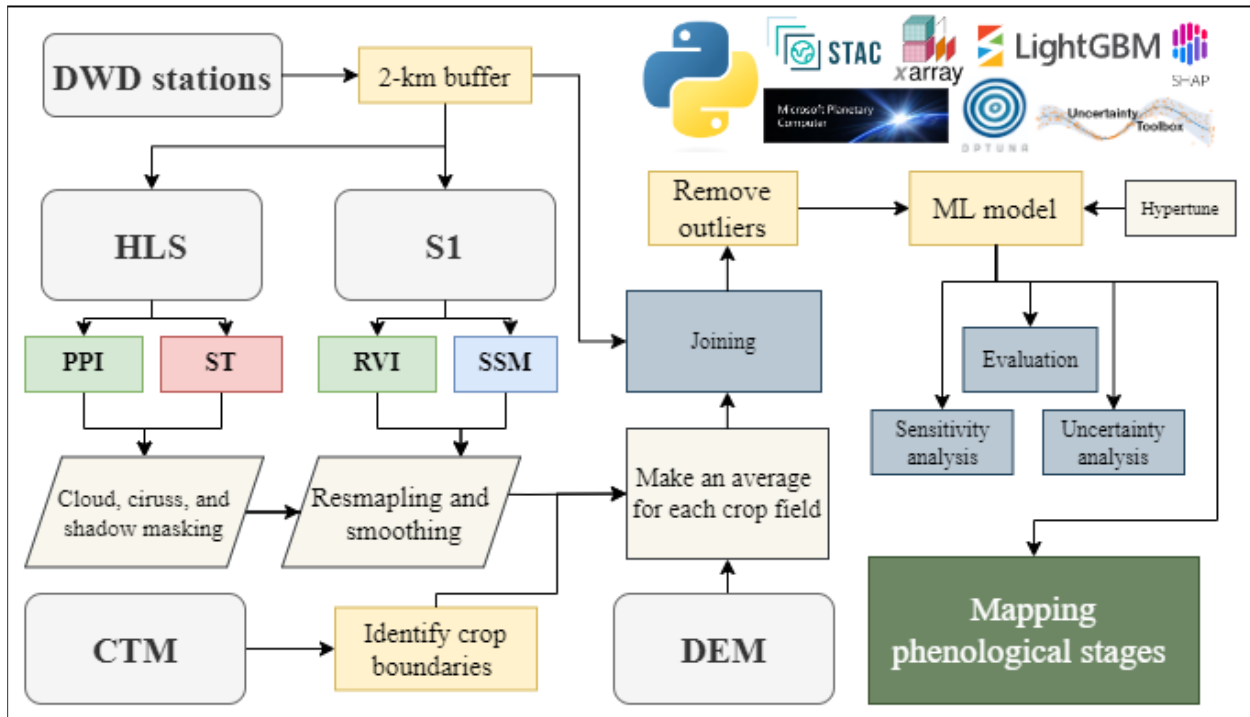


Figure 3: Flowchart of the proposed framework. All abbreviations are defined in the text.

## 3. Results and discussion

This study proposed a framework to estimate phenological developments of eight crops for 13 phenology stages across Germany at field scales of 30 m between 2017 and 2021. By fusing optical and radar datasets, this study assessed the effects of EO derived parameters on each crop and phenology stages (Section 3.1) and interpreted the impacts on crop phenology modeling using ML

model (Section 3.2). This study achieved highly accurate estimates of phenological development for eight different crops which are comparable in most cases and precise estimates in the start and the end of season compared to previous studies (Section 3.3). Nonetheless, model accuracy and uncertainty analysis revealed that the proposed framework displays a level of uncertainty in middle of season similar to previous studies (Section 3.4); however, it is important to mention that the proposed framework outperformed previous studies by a significant margin in terms of accuracy and certainty and it is accurate enough to be used for mapping phenology from local to national extents (Section 3.5). In the following sections, the proposed method is evaluated to address the objectives and questions of this study.

### 3.1. Feature selection

Several statistical analyses were carried out as part of a thorough analysis to assess how well each satellite image and parameter predicted phenology (Fig. 4). Using the non-dominated sorting genetic algorithm-III (NSGA-III, Fig. S5), a multi-objective sampling for hyper-tuning was carried out to confirm the efficacy of the suggested loss function. Results of optimization confirm that using single performance metric could lead to biased model; while proposed loss function (Section 2.7) showed its potential to reach a global optimum (Fig. S5) for hyper parameters of ML model. Relying on proposed loss function, it was discovered through examining the loss function values for every crop that multiple EO derived parameters are typically needed for precise phenology estimation, even though the patterns of loss function may differ between crops and BBCH stages. PPI had the lowest loss function values of all the single variables, indicating that it is a promising variable for phenology prediction. Furthermore, compared to SSM and ST, as and indirect factors that affect phenological development, RVI, as a direct measure that monitor plant phenology, is ranked as the second accurate indicator, as expected based on previous studies ([d'Andrimont et al. 2020](#); [Mercier et al. 2020](#)), to estimate phenology. However, when focusing on loss function, it is difficult to choose the ideal set of satellites and parameters, while it is evident that each crop requires a combination of parameters.

A specific analysis of the combined optical and SAR parameters using MCDM algorithms revealed that PPI-ST (which is best in 13% combinations of each crop and BBCH) and PPI-RVI-ST (26%) are among the best feature sets, studied for the most challenging phenology stage in BBCH equal 0 (~seeding, Fig. 4) based on previous studies ([d'Andrimont et al. 2020](#); [Lobert et al. 2023](#)).

Conover's test revealed that ST consistently exhibited the most significant difference from other feature sets which is in line with previous studies that showed soil temperature is significantly correlated with phenological development ([Fatima et al. 2020](#); [Zhang and Liu 2022](#)). This is highly plausible, since the main driver of phenology, are temperature sums, which are different for each crop and cultivar. Additionally, the combination of RVI and SSM consistently differentiated among crops and feature sets, confirming our initial hypothesis that utilizing SAR data solely with RVI might not adequately track phenological stages. Despite these findings, a definitive selection of the best feature set remains obscure, necessitating further investigation to establish a practical approach for mapping phenology by selecting the best candidate.

The results indicated that optical imagery typically outperforms SAR in phenology estimation across various crops and BBCH stages. However, no single optical combination emerges as the universally superior choice. This aligns with previous research, which has shown variable effectiveness of optical and SAR data depending on the crop, stage, and data fusion method employed ([Lobert et al. 2023](#); [Veloso et al. 2017](#)). For instance, [Mercier et al. \(2020\)](#) and [d'Andrimont et al. \(2020\)](#) reported superior accuracy of optical imagery over SAR in phenology estimation for winter wheat and rapeseed oil, respectively. Conversely, [Lobert et al. \(2023\)](#) found SAR to be more reliable for winter wheat phenology, while [Veloso et al. \(2017\)](#) advocated for a crop-specific and stage-specific approach to optical and SAR data utilization. Our results corroborate these findings, highlighting the superiority of optical (*i.e.*, PPI-ST) for estimating phenology stages for summer crops (maize, spring barley, spring oat, and sugar beet) at the beginning and end of the season (seeding, emergence, yellow ripeness, and harvesting) and PPI at in-season phenological stages ( $10 < \text{BBCH} < 87$ ). For winter crops, PPI-ST consistently outperforms SAR across all BBCH stages, making it the preferred combination for these crops. Therefore, optical imagery, particularly PPI-ST, emerges as the most accurate and versatile data source for phenology estimation across various crops and BBCH stages, with SAR offering less consistent performance in the study area. Even so, the fusion of optical and SAR parameters is outperforming PPI-ST for both summer and winter crops at different BBCHs. Yet, identifying the optimal feature set for modeling necessitates a deeper understanding of its underlying characteristics.



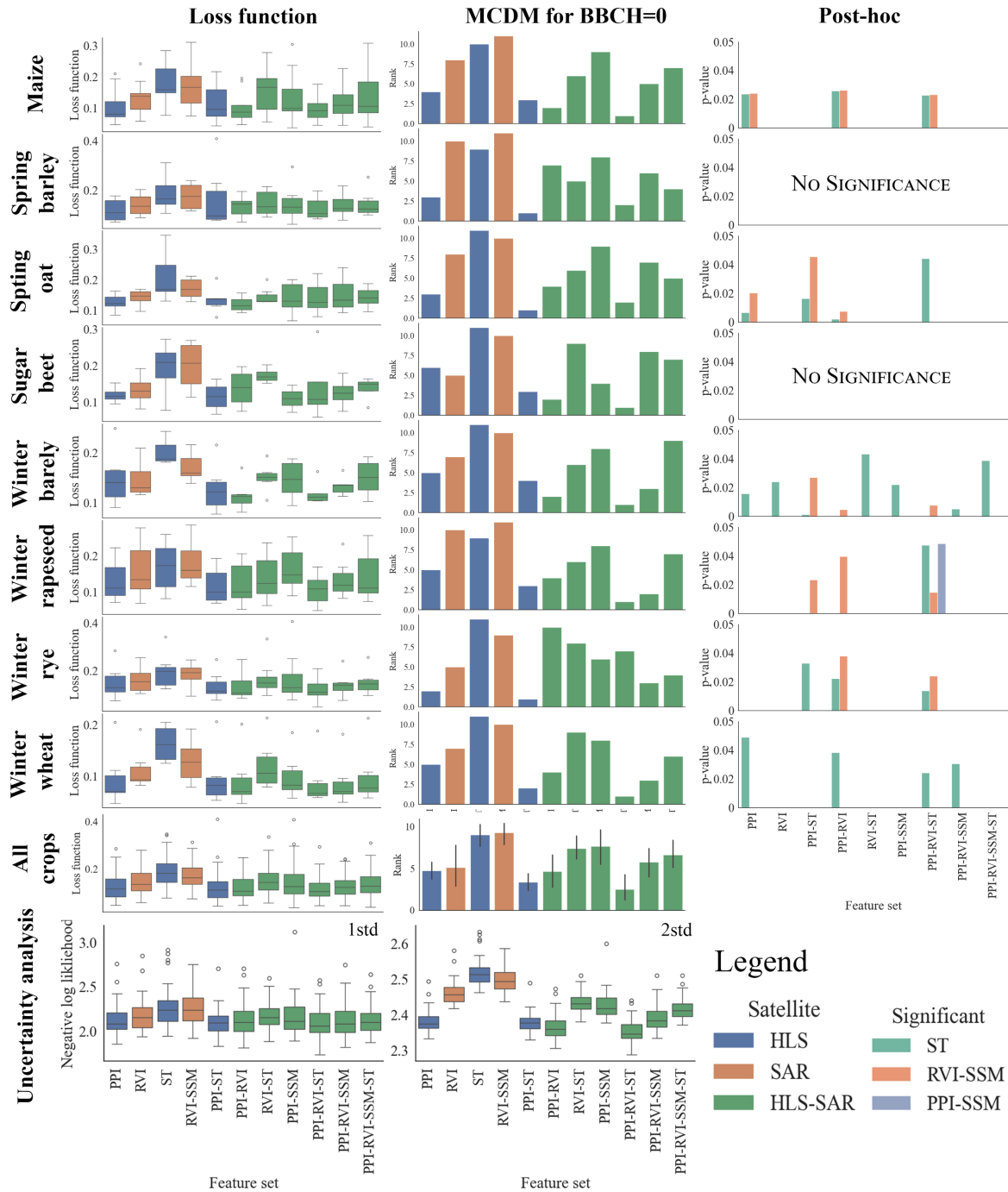


**Figure 4** Feature set comparison for each crop (left) loss function in hyper tuning process and each satellite data source (colors), (middle) MCDM selection for BBCH=0, (right) post-hoc analysis for significant test. The final row represents negative log likelihood of each feature sets (left) for one (middle) two (right) three standard deviations of uncertainty intervals.

Although ML models can yield precise estimations and valuable insights into target variables, they additionally come with some uncertainty. We examined the prediction intervals of every feature set for estimating phenology stages to obtain a better knowledge of this uncertainty. To obtain

accurate estimates of these intervals, we used conformal prediction using MAPIE agnostic model. negative log-likelihood, as an uncertainty metric, exhibited little variation across feature sets at the first standard deviation (roughly 68% of the uncertainty distribution), which mirrored the trends seen in the loss function except for RVI-SSM. It may be rooted in the fact that estimating SSM from SAR data results in deviations from real soil moisture ([van Hateren et al. 2023](#)). But the results show that PPI-ST and PPI-RVI-ST perform more effectively in estimating phenology stages at the second standard deviation (95% of the uncertainty distribution). Despite the relatively slight differences between these two combinations, PPI-RVI-ST continuously showed better agreement with observations based on the MCDM results for all crops and BBCH stages and will be the subject of further analysis in the following sections.

### **3.2. Feature importance and impact**

ML models' performances highly rely on the patterns and underlying information of input features. Thus, examining the relative importance of input features can provide valuable insights about physical interpretation of input parameters in ML models' outcome. As we expected from previous studies, ST ranked as the most important parameter in the model (Fig. 5A), while its impact varies depending on the value ranges. While lower values show negative SHAP values, higher ST values have a positive effect on the model output (SHAP values). In other words, higher ST values (mostly happens in bare soil before seeding and after harvesting) delays the target (day of the year), whereas smaller values with more significant opposite effects can rush the target). Further analysis showed aspect and slope came in second and third ranks of importance, supporting the well-known fact that slope and aspect has a direct impact on plant density and diversity; however, due to variations in location, crop type, and RS parameters, their impact within the ML model is not straightforward. Although PPI and RVI directly measure plant growth stages, feature importance analysis indicates that they have lower impacts on model variations. However, PPI and RVI have contrary effects based on SHAP values. This analysis shows the effect of each parameter on the final output of ML model, yet a deeper examination is necessary to completely understand the roles that each parameter in the ML model.

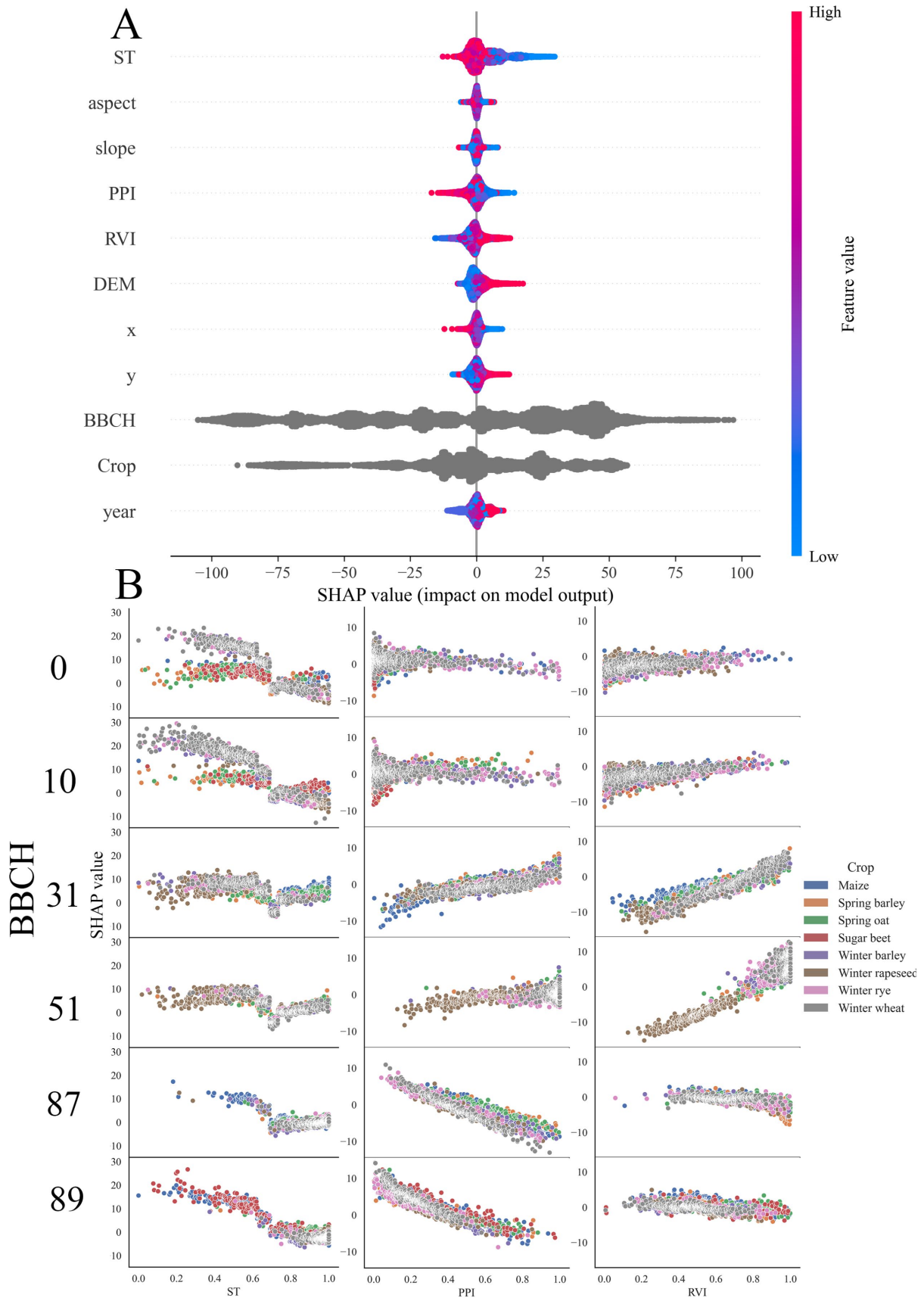


**Figure 5** SHAP values for different predictors and features. (A) Predictors are sorted based on the feature importance in the left, (B) SHAP values for each crop and BBCH are shown against (left) ST, (middle) PPI, and (right) RVI values.

More in depth analysis of EO derived parameters enabled us to assess the influences on ML model interpretations about each crop and BBCH. Thus, we evaluated the local SHAP values for ST, PPI, and RVI (Fig. 5B). The findings revealed that ST on the initial stages (BBCH 0 and 10) has a significant impact that suggests ST could be used as a valuable indicator for estimating the early stages of the growing season. This finding aligns with previous studies indicating that plants undergo active germination, emergence, and establishment during the early stages of the season are closely linked to temperature fluctuations ([Hatfield and Prueger 2015](#); [Ritchie and Nesmith 1991](#)). Despite the lower impact, ST at the harvesting stage (BBCH equal to 89) still exhibits a similar pattern to the early stages. This is due to the removal of crops, leaving behind bare soil and exposing it to direct sunlight, causing an increase in soil temperature. While soil temperature is a valuable indicator in the harvesting stage (BBCH 89), PPI emerges as a more effective indicator during the final stages of the season (BBCH 87 and 89), which is well aligned with previous studies ([Lobert et al. 2023](#); [Mercier et al. 2020](#)) that suggest optical imageries are more effective toward to end of the season. In addition, as [Jin and Eklundh \(2014\)](#) mentioned, PPI is affected by soil brightness at the start of the season and could not distinguish between vegetation and soil, due to a low amount of soil coverage by leaves. Therefore, as the ML model recognized patterns, PPI is not a good indicator for the start of the season. However, the rapid fluctuations in PPI following ripeness and harvesting (at the end of the season) facilitate the identification of phenological dates with greater precision by ML models. Additionally, PPI proves informative for phenological stages in the middle of the season (BBCH 31 and 51), albeit not to the same extent as RVI, as stated by [Meroni et al. \(2021\)](#) that more clear signals could be observe by SAR data compare to optical and optical data in heading stage. RVI stands out as an expert indicator for mid-season phenological stages and exerts a considerable influence on ML model. However, RVI and PPI is more reliable for winter rapeseed at BBCH 51, as confirmed by [d'Andrimont et al. \(2020\)](#), because it has a taller stature and a less dense canopy structure compared to other crops at this stage of development. Therefore, morphology of each crop plays a crucial role in detecting phenological stage developments. Future studies could consider exploring the impact of plant morphology on phenology estimations using EO data.

### 3.3. Model accuracy

The accuracy of the ML model is of paramount importance. As demonstrated in Fig. 6A, the model's accuracy is notable, with most predictions for all crops and BBCHs falling within a  $\pm 10$ -days interval of observed values, which is comparable with shape model fitting (SMF) ([Diao et al. 2021](#); [Liu et al. 2022a](#)) as one of the most recent and accurate methods on estimating phenological stages of crops, limited to places with observation when compared with our proposed method, which could be used to interpolate to places without observations (Section 3.5). This indicates the effectiveness of the proposed methodology in capturing patterns and trends from both RS and ground observations to accurately predict and map phenological stages. Moreover, the results reveal that all crops exhibit low bias and error metrics of RMSE and MAE which are consistently below 2 days. These findings underscore the well-tuned nature of the ML model, enabling precise phenological stage predictions across various crops and BBCH stages. Additionally, the distribution of residuals for each crop and BBCH is found to approximately follow a normal distribution, further confirming the model's robustness (Fig. S6). Although residuals are within  $\pm 10$  days, 60% of the residuals have lower than 1 day's difference and 99% are between -5 and 5 days for all crops and BBCHs. Thus, the proposed procedure to use stratified splitting for training and testing, along with stratified K-fold, resulted in a balanced model across different crops and BBCH stages, as opposed to using imbalanced data as an input.

To compare our model's performance with previous studies in Germany, we focused on winter wheat crop (Figure 6B). As evident from the results at unseen (test) data, our method consistently exhibits high accuracy and precision across all BBCH stages, except for BBCH 51 (heading), which exhibits a few outliers (residual  $> 5$  days). Despite these outliers, our method still achieves excellent precision, with an  $R^2$  value of 0.96 and a MAE of 1.18 days. Overall, our method outperforms previous studies in Germany, which have reported significantly higher errors ([Gerstmann et al. 2016](#); [Hoque 2022](#); [Lobert et al. 2023](#); [Yuan et al. 2021](#)). For instance, [Lobert et al. \(2023\)](#) obtained the lowest MAE of 4.5 days for the heading stage and the highest  $R^2$  value of 0.35. Their best results, achieved in the harvesting stage, yielded an  $R^2$  value of 0.62 and an MAE of 4.4 days. In comparison, our method achieved much higher agreement, with an  $R^2$  value of 0.98, and lower error, an MAE of 1.09 days. While both studies employed similar approaches, [Lobert et al. \(2023\)](#) deviated in two key aspects. Firstly, they employed a significantly high loess span parameter ( $= 0.3$ ), which drastically dampened peak values in time which imposes an uncertainty

by losing information through temporal variabilities. Additionally, they focused on raw data from satellite imageries while we used more physical-based and dependent RS indices and parameters. These two deviations could be contributed to their higher error rates and lower agreement with observations compared to our study.

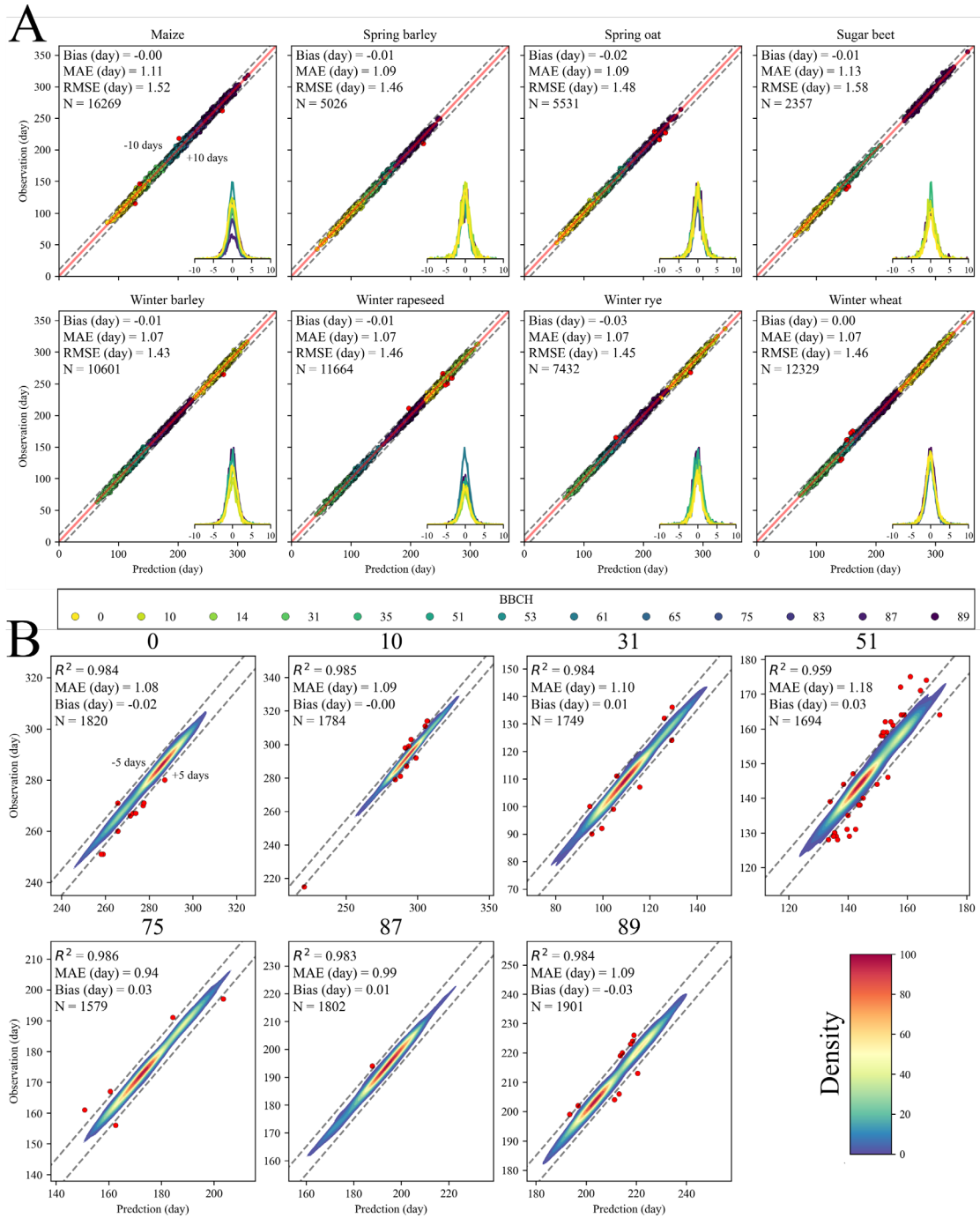


**Figure 6** Scatter plot of ten ensemble predictions versus observations for PPI-RVI-ST feature set (A) in each BBCH stage and crop type at unseen (test) data. The subplot in the lower right corner shows the residual probability distribution for each BBCH stage. (B) in each BBCH for winter wheat. Red points indicate stations where the difference between observations and predictions exceeds (A) 10 days, (B) 5 days. The numbers on each subplot of (B) are BBCH identifier [i.e., 0, 10, 31, 51, 75, 87, 89].



While our study closely resembles [Lobert et al. \(2023\)](#) in its utilization of RS data and fusion of multiple satellite datasets, several other studies have employed climate data or empirical/physical models for crop phenology estimation. For instance, [Gerstmann et al. \(2016\)](#) developed a statistical model to estimate/interpolate phenology across Germany for the same crops as our study. However, their model limitations preclude the consideration of seeding (BBCH~0) and harvesting (BBCH~89) stages. Comparison of our results with those of [Gerstmann et al. \(2016\)](#) reveals significant discrepancies across all BBCH stages and crops. The most accurate agreement of [Gerstmann et al. \(2016\)](#) study with an  $R^2$  of 0.89 for winter wheat emergence, still falls short of our  $R^2$  of 0.98. Similarly, while the RMSE of 2.14 for winter wheat heading phase in the [Gerstmann et al. \(2016\)](#) study is closer to our RMSE of 1.75, the  $R^2$  of 0.72 in their study stands in lower agreement to our 0.96. However, their model as they reported with spatial resolution of  $1 \times 1$  km based which predict phenology based on DEM and temperature has large uncertainties from temperature data, spatial resolution, and simplicity of model ([Gerstmann et al. 2016](#)).

On the other hand, conventional methods of phenology estimation based on LSP techniques, often struggle to accurately determine phenological stages towards the end of the growing season ([Meroni et al. 2021](#); [Tran et al. 2023](#)). Yet, our study corroborates findings by [Lobert et al. \(2023\)](#) and [Babcock et al. \(2021\)](#) that ML models could precisely identify end-of-season phenological stages. Although LSP models provide valuable insights about broad phenological trends and enable continental to global analysis of phenological developments, precise stage identification is crucial for precision agriculture. The proposed ML model successfully addresses this challenge, enabling accurate crop yield calibration and modeling at various stages of crop development from start to the end of growing season.

Several alternative approaches, including shape fitting models (SFMs) ([Sakamoto et al. 2010](#)) and hybrid phenology matching models ([Diao et al. 2021](#)), also have emerged to estimate phenological stages. These methods utilize procedures to fit and scale VIs derived from EO data with phenological observations collected across the United States (see [Diao et al. \(2021\)](#) for further details). Promising results have been reported with these methods, demonstrating high precision and low errors in estimating phenological stages, particularly when the VI time series is adjusted to account for spatial and temporal variations. Our approach aligns with these established methods, explicitly incorporating geolocation and year as input features for the ML model. For maize (corn)

at the planting (seeding) stage, our results exhibit comparable performance to those of [Diao et al. \(2021\)](#) for both the hybrid model ( $R^2 = 0.97$ ) and the SMF method ( $R^2 = 0.95$ ). Additionally, our method surpasses the hybrid model of [Diao et al. \(2021\)](#) by producing lower errors (RMSE = 1.93 versus 2.8). This evidence and previous comparison with previous studies further supports the effectiveness of our proposed method, which effectively integrates multiple approaches from ML model and VIs time series, to use time and space (geolocation and year) information as an input parameter for ML model to accurately estimate phenological stages.

### **3.4. Uncertainty analysis**

Various methods have been proposed to assess the uncertainty in ML models, including statistical techniques like ensemble methods and data-driven methods like quantile regression. In this study, we used both. Ensemble methods were employed to evaluate the uncertainty embedded in the ML models based on random initialization of hyperparameter optimization, data splitting, and cross-validation. Quantile regression was employed to make probabilistic ML model prediction intervals. Results show by using a simple averaging between ten ensemble models, the model is relatively precise in estimating phenological stages for various crops and BBCHs (Fig. 7A). In most cases, the prediction intervals compared to the range of the data are negligible. However, in terms of predictive uncertainty, the model does not show a perfect connection between standard deviation (computed as the standard deviation of predictions from ten ensemble models) and model residuals (difference between observation and estimation); yet a positive correlation and distributed residual close to zero can be observed. This finding suggests that the proposed ML model, with its input parameters, can predict uncertainty fairly (not perfectly), implying that the model is accurate enough in terms of uncertainty inherited from random initialization of the hyper tuning sampler but still it is a deterministic model. It means, in terms of uncertainty, the model is not perfectly predictive and needs to be optimized more deeply for predictive uncertainty and consider stochasticity of data. Future studies could focus on interpreting the inherent uncertainties arising from satellite noises, data collection procedures, and hyperparameter tuning as a valuable topic of investigation.

Quantile regression methods such as conformal predictions can be employed to generate probabilistic forecasts using ML models. We employed an agnostic model (MAPIE) capable of probabilistically predicting phenological stages (Fig. 7B). Our findings demonstrate that the ML

model can accurately predict phenological stages of winter wheat within a 5-day window, while the probability of a deviation exceeding 5 days is particularly low. The Mean Absolute Relative Percent Difference (MARPD) indicates highly accurate probabilistic forecasts (for probabilities greater than 0.95) for all phenological stages except BBCH 31. MARPD is below 1% for more than 95% of conditions, implying that the ML model can accurately predict phenological stages for most scenarios. Furthermore, additional uncertainty metrics such as the CHECK score (pinball loss) and the Continuous Ranked Probability Score (CRPS) confirm the ML model's ability to accurately assess uncertainty even for BBCH 31. The discrepancy between MARPD and other uncertainty metrics stems from MARPD's sensitivity to outliers, while the CHECK score and CRPS are less susceptible to outliers. Based on the uncertainty metrics, BBCH 31 exhibits more outliers compared to other stages, which aligns with [Lobert et al. \(2023\)](#) study. In comparison, the wide uncertainty intervals for BBCH 51 (heading) corroborate our prior findings from the regression analysis (Section 3.3), suggesting that the model faces the highest uncertainties and errors during heading stages in winter wheat.

### **3.5. Spatio-temporal analysis and mapping**

To evaluate the applicability and scalability of the proposed model, we assessed its ability to map phenological stages at local and national scales across Germany. To ensure the accuracy of the phenological maps, we continued our analysis for winter wheat for the geospatial variability of the model's phenological stage estimations at each DWD stations and BBCHs across the years (Fig. 8). The results determine the model's ability to accurately estimate phenological stages across Germany and different years, with some minor discrepancies observed for BBCH 51 at certain locations. Among all BBCHs, BBCH equal to 87 has the best accuracy, as it is reported by previous studies ([Gerstmann et al. 2016](#); [Lobert et al. 2023](#); [Meroni et al. 2021](#)). It is mainly because of the significant difference in color between yellow ripeness condition with previous stages, which is so clear and obvious from satellite imageries. It may relate to the drying of plants and decline in photosynthesis activities that could be obvious from optical imageries (but not SAR data as it is interpreted from feature analysis; Section 3.2). Moreover, the model presented consistent accuracy in phenological estimation across different years, including the drought year of 2018. These findings highlight the model's robustness and effectiveness in accurately predicting phenological stages throughout time and space. Additionally, our study in overall showed lower differences between predicted and observed data compared to [Lobert et al. \(2023\)](#). For example, in the best

case of their study in harvesting stage (BBCH=89), [Lobert et al. \(2023\)](#) had higher absolute differences with more than 20 days, while our study showed lower values with 7 days differences. This difference between this study and previous research could be found in each crop and BBCH stages. Thus, our model, to date, is the best model to predict the spatio-temporal variability of phenological developments.

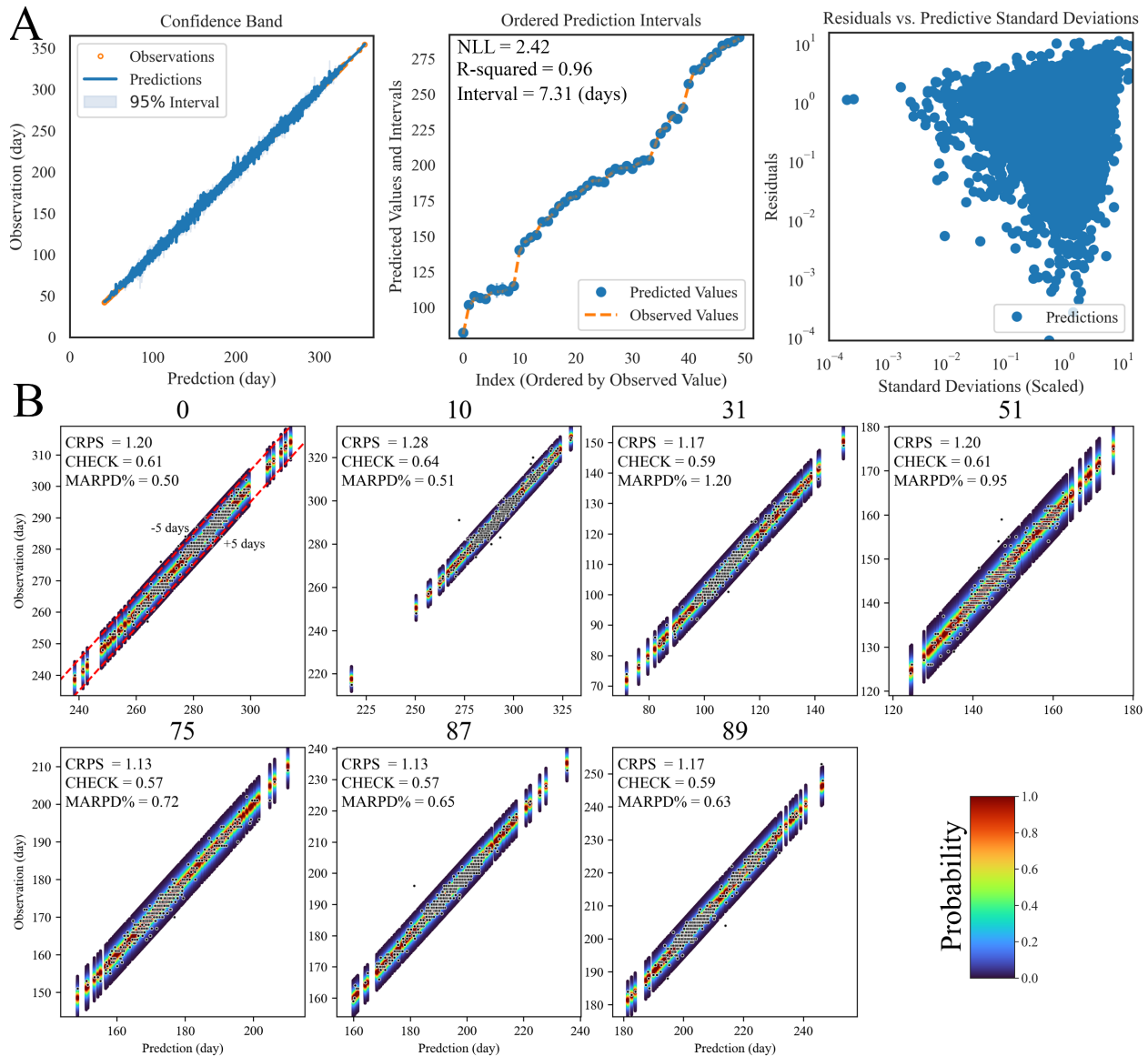


**Figure 7** Uncertainty analysis of PPI-RVI-ST feature set for all crop and BBCH (A) for ten ensembles averaging, (B) using conformal prediction method to construct a probabilistic estimate for winter wheat. The numbers on each subplot of (B) are BBCH identifier [i.e., 0, 10, 31, 51, 75, 87, 89].

To better understand the variations in phenological stages across different landscapes, we focused on a specific DWD station located in Empede, Neustadt, Lower Saxony with significant diversity in input data which has been used in ML model (e.g., altitude, crop types, and EO derived parameters), making it an ideal location for testing our model's ability to estimate phenological developments. Our results demonstrate that the model consistently and homogeneously predicts phenological stages for various crops and growth stages, even for challenging conditions like the drought year of 2018. Although in first sight it seems that the BBCH of 51 is more homogeneous, the BBCH of 0 and 10 are more precise on phenology estimation as they follow more closely the CTM patterns. This suggests that our model effectively captures the temporal dynamics of phenological stages while maintaining consistency within individual fields, especially in the start and end of season. Some discrepancies in phenological stage estimations may arise from the spatial resolution of the data (either in RS or CTM data) or uncertainties in the DWD observations.

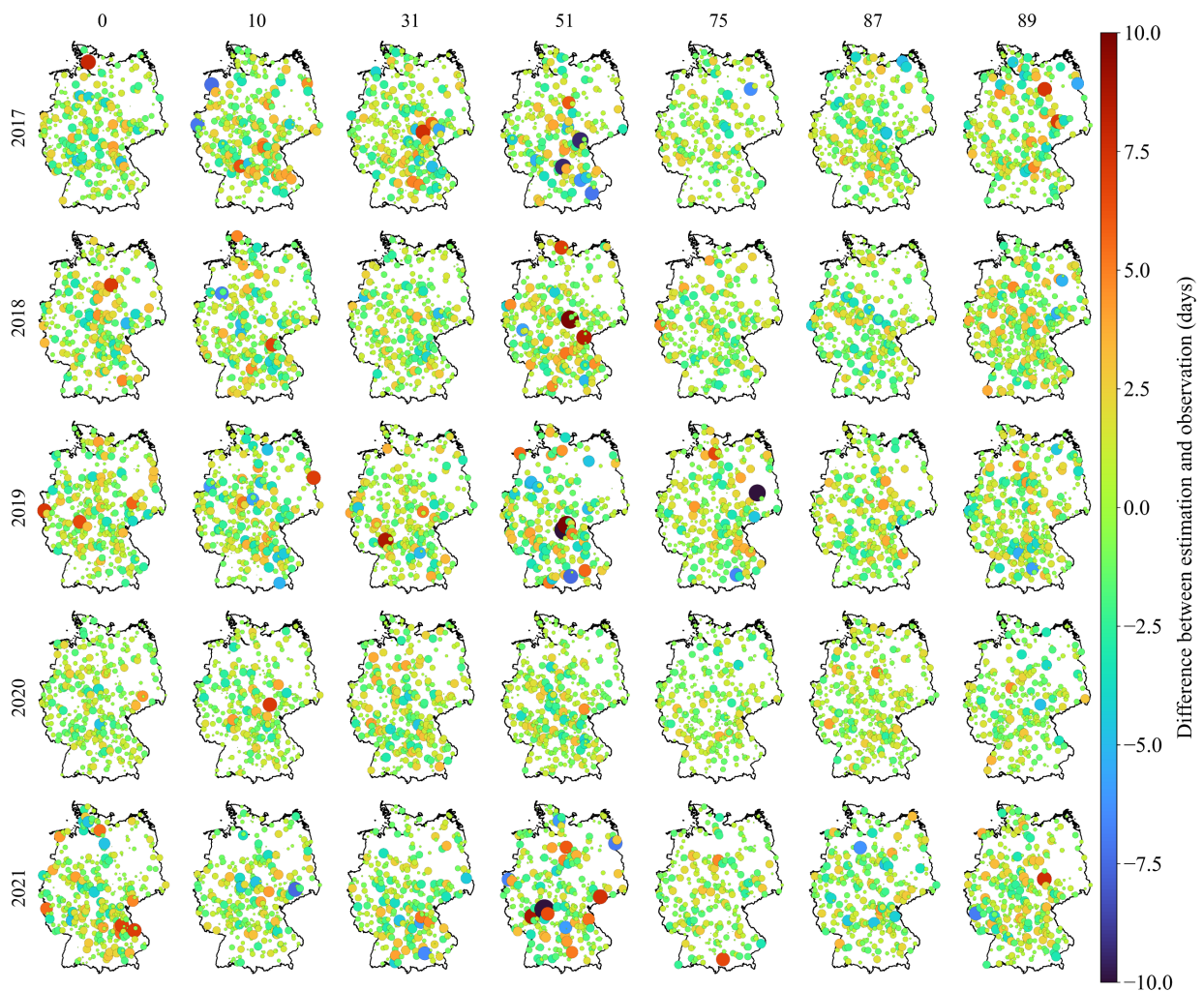


**Figure 8** Spatio-temporal difference between estimated and observed phenology for winter wheat across Germany. The color shows the difference amount and the size depended to the absolute difference between estimated and observed values. The numbers on top of each column are BBCH identifier [i.e., 0, 10, 31, 51, 75, 87, 89].

The proposed ML model is estimating probability distributions of phenological stages based on time series of parameters derived from EO data time series (Fig. 9B). It means ML model estimates a range of dates for each value of time series. Therefore, the most probable date should be extracted from time series to represent the exact date of each phenological stage. Various statistical aggregators through the time such as mean, median, and mode are evaluated, and it was discovered that the median could be an efficient way to represent phenological stages. It may be rooted in the usage of median aggregation within 2-kilometer buffers of DWD stations to construct the training dataset from EO and observation data. The probability distributions reveal that the model is a bit uncertain about the middle of season compared to start and end of the season, which is well aligned with our previous findings on both model accuracy and uncertainty analysis sections. Although our study estimate lower probabilities for each phenological stages compared to [Lobert et al. \(2023\)](#), the range of estimated days of the year is narrower. It may be attributed to several reasons such as modeling procedure (hyper tuning of ML model), resampling and smoothing of EO derived time series (preserving peak values), number of observations (>150,000), and considering space and time factors as input data (geolocation and year).



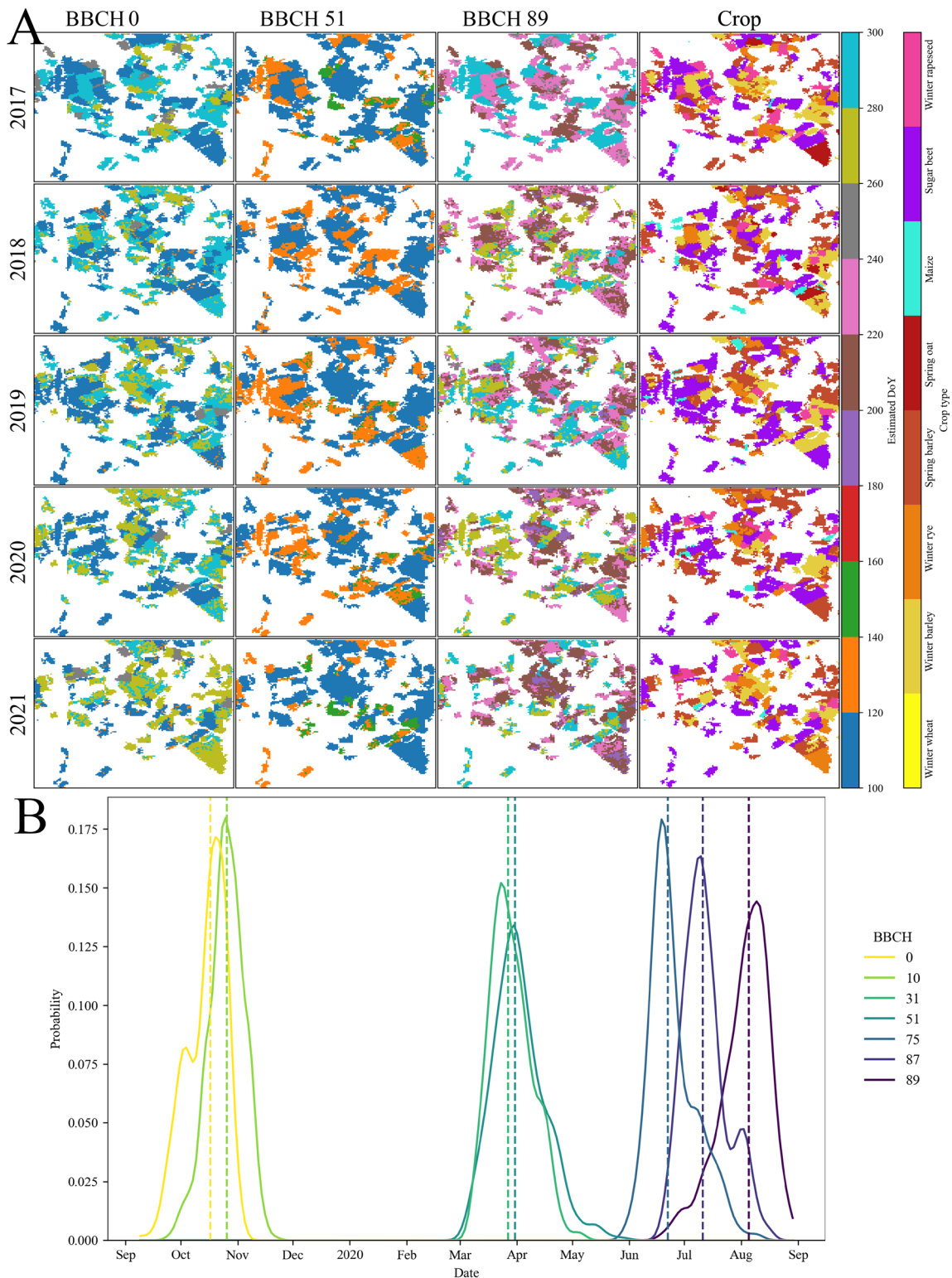


**Figure 9** (A) Spatio-temporal map of phenology for three major BBCHs of start of the season (seeding~BBCH=0), middle of season (heading~BBCH=51), and end of season (harvest~BBCH=89) at Empede, Neustadt, Lower Saxony. (B) Probability of phenological stages estimated by time series of EO data for winter wheat fields at Empede, Neustadt, Lower Saxony. Note: dashed lines are the median of phenological stages at each BBCHs.



### 3.6. Study limitations

We shaped our study based on DWD observations collected by trained volunteers across Germany. Like any observation, aleatoric uncertainties (here human errors) occur during the data gathering process (here, field observation) are an inevitable part ([Liu et al. 2021](#)). For instance, some of the sampling points had insufficient location precision (locations with 1 decimal precision; for example, 4.4 as a longitude of a DWD station, which is not precise enough for pixel accuracy of 30 m in this study). Therefore, not only the aleatoric sampling uncertainty affecting the reference data (known as human error) but also sampling strategy are not established/reported observation points with required precision in some cases.

On the other hand, the pixel size issues (known as footprint mismatch between observations and EO data) in RS application is always a common issue which could affect modeling accuracy and impose undesirable uncertainties, especially when focusing on time series modeling ([Povey and Grainger 2015](#)). Additionally, because we are fusing SAR data of 10 m resolution with Landsat and Sentinel-2 of 30 m resolution, we forced to upscale SAR to HLS. We used an average upscaling approach, as it is known that imposes lower errors in geographic information systems (GIS) procedures. Also, footprint mismatch can affect the boundaries of different crop fields, which is substantially changes the map of phenological developments like its effects on land cover mapping ([Lechner et al. 2009](#)). This footprint mismatch is also available in CTM data, as it is shown in Section 2.4.

The biases and uncertainties in EO data are not solely related to pixel size. Various factors such as climate condition, cloud coverage, accuracy of cloud removal, and especially the noises in time series modeling based on EO data could relatively affect the modeling precision ([Li et al. 2022b](#); [Zhou et al. 2016](#)). Additionally, the noise reduction procedure is always affecting the peak values of agricultural indices (e.g., NVDI) and could introduce uncertainties to modeling process. This point can affect the precision more than cited issues ([Shao et al. 2016](#)). Although we proposed an approach to first resample RS time series to weekly and then use small suppression coefficient for smoothing, we still lost some information about real peak values, yet we deem this not substantial. However, this could decrease the modeling accuracy in the middle of the season, as perceivable in our study (Sections 3.3 and 3.4) and commonly by other researches ([Gerstmann et al. 2016](#); [Lobert et al. 2023](#)).

#### 4. Summary and conclusion

In this study we evaluated the fusion of optical and SAR imageries integrated with an ML model to estimate phenological development for eight crops and 13 plant growth stages across Germany. We used diverse physically-based EO indices and parameters from various satellites to explore the efficiency of combining multiple RS parameters on the precision of a proposed ML model. We further improved our ML model accuracy using hyper tuning approach and proposing multiple feature set based on satellites and parameters to understand underlying characteristics. To better understand the ML model interpretability, we used a local and global sensitivity analysis based on SHAP values. We also conducted an uncertainty analysis using various methods of ensemble modeling and quantile regression.

Satellite parameters and phenological observations of DWD stations were arranged to create a training dataset to build and calibrate an ML model with the aim to predict phenological development of selected crops across Germany. To evaluate the ML model's accuracy, we split data using stratified procedure based on crop type and phenological stages (BBCH) to 60% of training, 20% of validation, and 20% of a test (unseen) data. The results indicate that the proposed ML model with  $RMSE < 1.6$ ,  $MAE < 1.15$  and  $bias \approx 0$  (days) on estimating phenological developments for all crops had excellent precision with minor deficiency in the middle of the season (heading) compared to other phenological stages. Additionally, the proposed model could effectively find spatio-temporal variability and patterns of phenological developments across Germany. However, in terms of uncertainty analysis, even though the model could capture probable uncertainties, it is not as predictive as the deterministic; however, in terms of uncertainty metrics of negative log-likelihood  $< 2.42$  it is predictive enough as a deterministic model.

The findings and probable future study objectives are summarized as follows:

- 1- Preprocessing approaches to prepare input data for ML models need to be carefully performed, especially when EO-based time series are resampled to larger temporal resolutions and smoothed to remove noises from various sources.
- 2- Hyper tuning of ML model is a necessary step to find and fairly compare the potential of each satellite in estimating phenological developments.

- 3- Feature selection analysis indicates that selecting combined feature sets from multiple satellites does not have a straightforward pathway and needs in depth analysis about various aspects of modeling approach.
- 4- Feature interpretation needs advanced analysis tools such as SHAP to understand the cognition process of ML model based on input features.
- 5- ML models are useful and precise to estimate phenological stages of crops using EO data when hyper tuned and calibrated well.
- 6- Proposing loss function based on various performance metrics for hyper tuning could improve modeling efficiency and better calibrate model parameters.
- 7- When data is imbalanced for various crops and BBCHs, stratified sampling and splitting for modeling is necessary to calibrate ML model efficiently.
- 8- It is ideal to propose an ML modeling pipeline to prepare the required information for phenological estimation based on proposed EO-based indices, particularly here addressing crop type mapping from EO data.
- 9- In future studies, it is more appropriate to calibrate model not only for performance metrics but also for uncertainty metrics such as negative log-likelihood, to be more predictive about uncertainties. We suggest quantile regression methods, which guarantee mathematically to produce reliable forecasts.

## **Funding**

This research was funded by the joint project of Digitalization in organic agriculture (DigiPlus)-subproject A (grant no. 28 DE 207 A 21).

## **Data availability**

All data sources used in this study are available freely. HLS dataset is available through STAC (<https://cmr.earthdata.nasa.gov/stac/LPCLOUD>), Sentinel-1 through MPC STAC (<https://planetarycomputer.microsoft.com/api/stac/v1/>), FABDEM through GEE community catalog (<https://gee-community-catalog.org/projects/fabdem/>), and DWD observations through website ([https://opendata.dwd.de/climate\\_environment/CDC/observations\\_germany/phenology/](https://opendata.dwd.de/climate_environment/CDC/observations_germany/phenology/)). PhenoMapper, online web application, is also prepared to easily present phenological maps across Germany (<https://ee-shahab2710.projects.earthengine.app/view/phenomapper>).

## References

- Akiba, T., Sano, S., Yanase, T., Ohta, T., & Koyama, M. (2019). Optuna: A Next-generation Hyperparameter Optimization Framework. In *Proceedings of the 25th ACM SIGKDD International Conference on Knowledge Discovery & Data Mining* (pp. 2623–2631). Anchorage, AK, USA: Association for Computing Machinery
- Angelopoulos, A.N., & Bates, S. (2021). A gentle introduction to conformal prediction and distribution-free uncertainty quantification. *arXiv preprint arXiv:2107.07511*
- Babcock, C., Finley, A.O., & Looker, N. (2021). A Bayesian model to estimate land surface phenology parameters with harmonized Landsat 8 and Sentinel-2 images. *Remote Sensing of Environment*, *261*, 112471
- Badeck, F.W., Bondeau, A., Böttcher, K., Doktor, D., Lucht, W., Schaber, J., & Sitch, S. (2004). Responses of spring phenology to climate change. *New Phytologist*, *162*, 295-309
- Bauer-Marschallinger, B., Freeman, V., Cao, S., Paulik, C., Schaufler, S., Stachl, T., Modanesi, S., Massari, C., Ciabatta, L., Brocca, L., & Wagner, W. (2019). Toward Global Soil Moisture Monitoring With Sentinel-1: Harnessing Assets and Overcoming Obstacles. *IEEE Transactions on Geoscience and Remote Sensing*, *57*, 520-539
- Blickensdorfer, L., Schwieder, M., Pflugmacher, D., Nendel, C., Erasmi, S., & Hostert, P. (2022). Mapping of crop types and crop sequences with combined time series of Sentinel-1, Sentinel-2 and Landsat 8 data for Germany. *Remote Sensing of Environment*, *269*, 112831
- Brans, J.P., Vincke, P., & Mareschal, B. (1986). How to Select and How to Rank Projects - the Promethee Method. *European journal of operational research*, *24*, 228-238
- Canisius, F., Shang, J.L., Liu, J.G., Huang, X.D., Ma, B.L., Jiao, X.F., Geng, X.Y., Kovacs, J.M., & Walters, D. (2018). Tracking crop phenological development using multi-temporal polarimetric Radarsat-2 data. *Remote Sensing of Environment*, *210*, 508-518
- Chen, T., & Guestrin, C. (2016). Xgboost: A scalable tree boosting system. In *Proceedings of the 22nd acm sigkdd international conference on knowledge discovery and data mining* (pp. 785-794)
- Chung, Y., Char, I., Guo, H., Schneider, J., & Neiswanger, W. (2021). Uncertainty toolbox: an open-source library for assessing, visualizing, and improving uncertainty quantification. *arXiv preprint arXiv:2109.10254*
- Claverie, M., Ju, J., Masek, J.G., Dungan, J.L., Vermote, E.F., Roger, J.C., Skakun, S.V., & Justice, C. (2018). The Harmonized Landsat and Sentinel-2 surface reflectance data set. *Remote Sensing of Environment*, *219*, 145-161
- Conover, W.J., & Iman, R.L. (1981). Rank transformations as a bridge between parametric and nonparametric statistics. *The American Statistician*, *35*, 124-129
- Czernecki, B., Nowosad, J., & Jablonska, K. (2018). Machine learning modeling of plant phenology based on coupling satellite and gridded meteorological dataset. *Int J Biometeorol*, *62*, 1297-1309
- d'Andrimont, R., Taymans, M., Lemoine, G., Ceglar, A., Yordanov, M., & van der Velde, M. (2020). Detecting flowering phenology in oil seed rape parcels with Sentinel-1 and -2 time series. *Remote Sensing of Environment*, *239*, 111660
- Dandabathula, G., Hari, R., Ghosh, K., Bera, A.K., & Srivastav, S.K. (2023). Accuracy assessment of digital bare-earth model using ICESat-2 photons: analysis of the FABDEM. *Modeling Earth Systems and Environment*, *9*, 2677-2694
- Diao, C.Y., Yang, Z.J., Gao, F., Zhang, X.Y., & Yang, Z.W. (2021). Hybrid phenology matching model for robust crop phenological retrieval. *ISPRS Journal of Photogrammetry and Remote Sensing*, *181*, 308-326

- Falkner, S., Klein, A., & Hutter, F. (2018). BOHB: Robust and efficient hyperparameter optimization at scale. In *International conference on machine learning* (pp. 1437-1446): PMLR
- Fatima, Z., Ahmed, M., Hussain, M., Abbas, G., Ul-Allah, S., Ahmad, S., Ahmed, N., Ali, M.A., Sarwar, G., Haque, E.u., Iqbal, P., & Hussain, S. (2020). The fingerprints of climate warming on cereal crops phenology and adaptation options. *Scientific Reports*, *10*, 18013
- Gao, Y., Wang, L.G., Zhong, G.J., Wang, Y.T., & Yang, J.H. (2023). Potential of Remote Sensing Images for Soil Moisture Retrieving Using Ensemble Learning Methods in Vegetation-Covered Area. *IEEE Journal of Selected Topics in Applied Earth Observations and Remote Sensing*, *16*, 8149-8165
- Gerstmann, H., Doktor, D., Glässer, C., & Möller, M. (2016). PHASE: A geostatistical model for the Kriging-based spatial prediction of crop phenology using public phenological and climatological observations. *Computers and Electronics in Agriculture*, *127*, 726-738
- Gupta, H.V., Kling, H., Yilmaz, K.K., & Martinez, G.F. (2009). Decomposition of the mean squared error and NSE performance criteria: Implications for improving hydrological modelling. *Journal of Hydrology*, *377*, 80-91
- Guth, P.L., & Geoffroy, T.M. (2021). LiDAR point cloud and ICESat-2 evaluation of 1 second global digital elevation models: Copernicus wins. *Transactions in GIS*, *25*, 2245-2261
- Hatfield, J.L., & Prueger, J.H. (2015). Temperature extremes: Effect on plant growth and development. *Weather and Climate Extremes*, *10*, 4-10
- Hawker, L., Uhe, P., Paulo, L., Sosa, J., Savage, J., Sampson, C., & Neal, J. (2022). A 30 m global map of elevation with forests and buildings removed. *Environmental Research Letters*, *17*, 024016
- Holzworth, D.P., Huth, N.I., deVoil, P.G., Zurcher, E.J., Herrmann, N.I., McLean, G., Chenu, K., van Oosterom, E.J., Snow, V., Murphy, C., Moore, A.D., Brown, H., Whish, J.P.M., Verrall, S., Fainges, J., Bell, L.W., Peake, A.S., Poulton, P.L., Hochman, Z., Thorburn, P.J., Gaydon, D.S., Dalglish, N.P., Rodriguez, D., Cox, H., Chapman, S., Doherty, A., Teixeira, E., Sharp, J., Cichota, R., Vogeler, I., Li, F.Y., Wang, E., Hammer, G.L., Robertson, M.J., Dimes, J.P., Whitbread, A.M., Hunt, J., van Rees, H., McClelland, T., Carberry, P.S., Hargreaves, J.N.G., MacLeod, N., McDonald, C., Harsdorf, J., Wedgwood, S., & Keating, B.A. (2014). APSIM – Evolution towards a new generation of agricultural systems simulation. *Environmental Modelling & Software*, *62*, 327-350
- Hoque, A. (2022). Variability of wheat phenology from Sentinel-1 and -2 time series : a case study for Brandenburg, Germany. In
- Hwang, C.-L., Yoon, K., Hwang, C.-L., & Yoon, K. (1981). Methods for multiple attribute decision making. *Multiple attribute decision making: methods and applications a state-of-the-art survey*, 58-191
- Ishizaka, A., & Nemery, P. (2013). *Multi-criteria decision analysis: methods and software*. John Wiley & Sons
- Jin, H.X., & Eklundh, L. (2014). A physically based vegetation index for improved monitoring of plant phenology. *Remote Sensing of Environment*, *152*, 512-525
- Kaspar, F., Zimmermann, K., & Polte-Rudolf, C. (2015). An overview of the phenological observation network and the phenological database of Germany's national meteorological service (Deutscher Wetterdienst). *Advances in Science and Research*, *11*, 93-99
- Katal, N., Rzanny, M., Mader, P., & Waldchen, J. (2022). Deep Learning in Plant Phenological Research: A Systematic Literature Review. *Front Plant Sci*, *13*, 805738
- Ke, G., Meng, Q., Finley, T., Wang, T., Chen, W., Ma, W., Ye, Q., & Liu, T.-Y. (2017). LightGBM: A Highly Efficient Gradient Boosting Decision Tree. In *Neural Information Processing Systems*

Khabbazan, S., Steele-Dunne, S.C., Vermunt, P., Judge, J., Vreugdenhil, M., & Gao, G. (2022). The influence of surface canopy water on the relationship between L-band backscatter and biophysical variables in agricultural monitoring. *Remote Sensing of Environment*, 268, 112789

Kizielewicz, B., Shekhovtsov, A., & Sałabun, W. (2023). pymcdm—The universal library for solving multi-criteria decision-making problems. *SoftwareX*, 22, 101368

Kooistra, L., Berger, K., Brede, B., Graf, L.V., Aasen, H., Roujean, J.-L., Machwitz, M., Schlerf, M., Atzberger, C., & Prikaziuk, E. (2023). Reviews and syntheses: Remotely sensed optical time series for monitoring vegetation productivity. *Biogeosciences Discussions*, 2023, 1-67

Kowalski, K., Senf, C., Hostert, P., & Pflugmacher, D. (2020). Characterizing spring phenology of temperate broadleaf forests using Landsat and Sentinel-2 time series. *International Journal of Applied Earth Observation and Geoinformation*, 92, 102172

Lechner, A.M., Stein, A., Jones, S.D., & Ferwerda, J.G. (2009). Remote sensing of small and linear features: Quantifying the effects of patch size and length, grid position and detectability on land cover mapping. *Remote Sensing of Environment*, 113, 2194-2204

Li, H., Zhao, J.Y., Yan, B.Q., Yue, L.W., & Wang, L.C. (2022a). Global DEMs vary from one to another: an evaluation of newly released Copernicus, NASA and AW3D30 DEM on selected terrains of China using ICESat-2 altimetry data. *International Journal of Digital Earth*, 15, 1149-1168

Li, R.M., Xia, H.M., Zhao, X.Y., & Guo, Y. (2023). Mapping evergreen forests using new phenology index, time series Sentinel-1/2 and Google Earth Engine. *Ecological Indicators*, 149, 110157

Li, W.J., Xin, Q.C., Zhou, X.W., Zhang, Z.C., & Ruan, Y.J. (2021). Comparisons of numerical phenology models and machine learning methods on predicting the spring onset of natural vegetation across the Northern Hemisphere. *Ecological Indicators*, 131, 108126

Li, Z., Shen, H., Weng, Q., Zhang, Y., Dou, P., & Zhang, L. (2022b). Cloud and cloud shadow detection for optical satellite imagery: Features, algorithms, validation, and prospects. *ISPRS Journal of Photogrammetry and Remote Sensing*, 188, 89-108

Liu, G., Chuine, I., Denéchére, R., Jean, F., Dufrêne, E., Vincent, G., Berveiller, D., & Delpierre, N. (2021). Higher sample sizes and observer inter-calibration are needed for reliable scoring of leaf phenology in trees. *Journal of Ecology*, 109, 2461-2474

Liu, H., Zhou, B., Bai, Z., Zhao, W., Zhu, M., Zheng, K., Yang, S., & Li, G. (2023). Applicability Assessment of Multi-Source DEM-Assisted InSAR Deformation Monitoring Considering Two Topographical Features. In, *Land*

Liu, L.C., Cao, R.Y., Chen, J., Shen, M.G., Wang, S., Zhou, J., & He, B.B. (2022a). Detecting crop phenology from vegetation index time-series data by improved shape model fitting in each phenological stage. *Remote Sensing of Environment*, 277, 113060

Liu, Z.C., Fu, Y.H., Shi, X.R., Lock, T.R., Kallenbach, R.L., & Yuan, Z.Y. (2022b). Soil moisture determines the effects of climate warming on spring phenology in grasslands. *Agricultural and Forest Meteorology*, 323, 109039

Lobert, F., Löw, J., Schwieder, M., Gocht, A., Schlund, M., Hostert, P., & Erasmi, S. (2023). A deep learning approach for deriving winter wheat phenology from optical and SAR time series at field level. *Remote Sensing of Environment*, 298, 113800

Lundberg, S.M., & Lee, S.I. (2017). A Unified Approach to Interpreting Model Predictions. *Advances in Neural Information Processing Systems 30 (Nips 2017)*, 30

- Ma, Y.Y., Shen, Y.L., Guan, H.X., Wang, J., & Hu, C.L. (2023). A novel approach to detect the spring corn phenology using layered strategy. *International Journal of Applied Earth Observation and Geoinformation*, *122*, 103422
- MacBean, N., Maignan, F., Peylin, P., Bacour, C., Bréon, F.M., & Ciais, P. (2015). Using satellite data to improve the leaf phenology of a global terrestrial biosphere model. *Biogeosciences*, *12*, 7185-7208
- Mandal, D., Ratha, D., Bhattacharya, A., Kumar, V., McNairn, H., Rao, Y.S., & Frery, A.C. (2020). A Radar Vegetation Index for Crop Monitoring Using Compact Polarimetric SAR Data. *IEEE Transactions on Geoscience and Remote Sensing*, *58*, 6321-6335
- Marini, L., Scotton, M., Klimek, S., Isselstein, J., & Pecile, A. (2007). Effects of local factors on plant species richness and composition of Alpine meadows. *Agriculture Ecosystems & Environment*, *119*, 281-288
- Marsh, C.B., Harder, P., & Pomeroy, J.W. (2023). Validation of FABDEM, a global bare-earth elevation model, against UAV-lidar derived elevation in a complex forested mountain catchment. *Environmental Research Communications*, *5*, 031009
- Massey Jr, F.J. (1951). The Kolmogorov-Smirnov test for goodness of fit. *Journal of the American statistical Association*, *46*, 68-78
- Mercier, A., Betbeder, J., Baudry, J., Le Roux, V., Spicher, F., Lacoux, J., Roger, D., & Hubert-Moy, L. (2020). Evaluation of Sentinel-1 & 2 time series for predicting wheat and rapeseed phenological stages. *ISPRS Journal of Photogrammetry and Remote Sensing*, *163*, 231-256
- Meroni, M., d'Andrimont, R., Vrieling, A., Fasbender, D., Lemoine, G., Rembold, F., Seguini, L., & Verhegghen, A. (2021). Comparing land surface phenology of major European crops as derived from SAR and multispectral data of Sentinel-1 and -2. *Remote Sens Environ*, *253*, 112232
- Morellato, L.P.C., Alberton, B., Alvarado, S.T., Borges, B., Buisson, E., Camargo, M.G.G., Cancian, L.F., Carstensen, D.W., Escobar, D.F.E., Leite, P.T.P., Mendoza, I., Rocha, N.M.W.B., Soares, N.C., Silva, T.S.F., Staggemeier, V.G., Streher, A.S., Vargas, B.C., & Peres, C.A. (2016). Linking plant phenology to conservation biology. *Biological Conservation*, *195*, 60-72
- Nash, J.E., & Sutcliffe, J.V. (1970). River flow forecasting through conceptual models part I — A discussion of principles. *Journal of Hydrology*, *10*, 282-290
- Nietupski, T.C., Kennedy, R.E., Temesgen, H., & Kerns, B.K. (2021). Spatiotemporal image fusion in Google Earth Engine for annual estimates of land surface phenology in a heterogeneous landscape. *International Journal of Applied Earth Observation and Geoinformation*, *99*, 102323
- Peano, D., Hemming, D., Materia, S., Delire, C., Fan, Y., Joetzjer, E., Lee, H., Nabel, J.E.M.S., Park, T., Peylin, P., Wårlind, D., Wiltshire, A., & Zaehle, S. (2021). Plant phenology evaluation of CRESCENDO land surface models – Part 1: Start and end of the growing season. *Biogeosciences*, *18*, 2405-2428
- Pipia, L., Munoz-Mari, J., Amin, E., Belda, S., Camps-Valls, G., & Verrelst, J. (2019). Fusing optical and SAR time series for LAI gap filling with multioutput Gaussian processes. *Remote Sens Environ*, *235*
- Povey, A.C., & Grainger, R.G. (2015). Known and unknown unknowns: uncertainty estimation in satellite remote sensing. *Atmos. Meas. Tech.*, *8*, 4699-4718
- Ritchie, J.T., & Nasmith, D.S. (1991). Temperature and crop development. *Modeling plant and soil systems*, *31*, 5-29
- Sakamoto, T., Wardlow, B.D., Gitelson, A.A., Verma, S.B., Suyker, A.E., & Arkebauer, T.J. (2010). A Two-Step Filtering approach for detecting maize and soybean phenology with time-series MODIS data. *Remote Sensing of Environment*, *114*, 2146-2159



- Savitzky, A., & Golay, M.J.E. (2002). Smoothing and Differentiation of Data by Simplified Least Squares Procedures. *Analytical Chemistry*, 36, 1627-1639
- Schwartz, M.D. (2003). *Phenology: an integrative environmental science*. Springer
- Shao, Y., Lunetta, R.S., Wheeler, B., Iames, J.S., & Campbell, J.B. (2016). An evaluation of time-series smoothing algorithms for land-cover classifications using MODIS-NDVI multi-temporal data. *Remote Sensing of Environment*, 174, 258-265
- Shapiro, S.S., & Wilk, M.B. (1965). An analysis of variance test for normality (complete samples). *Biometrika*, 52, 591-611
- Shimada, M., Itoh, T., Motooka, T., Watanabe, M., Shiraishi, T., Thapa, R., & Lucas, R. (2014). New global forest/non-forest maps from ALOS PALSAR data (2007–2010). *Remote Sensing of Environment*, 155, 13-31
- Singh, S. (2018). Understanding the role of slope aspect in shaping the vegetation attributes and soil properties in Montane ecosystems. *Tropical Ecology*, 59, 417-430
- Small, D. (2011). Flattening Gamma: Radiometric Terrain Correction for SAR Imagery. *IEEE Transactions on Geoscience and Remote Sensing*, 49, 3081-3093
- Source, M.O., McFarland, M., Emanuele, R., Morris, D., & Augspurger, T. (2022). microsoft/PlanetaryComputer: October 2022. In: Zenodo
- Stöckli, R., & Vidale, P.L. (2004). European plant phenology and climate as seen in a 20-year AVHRR land-surface parameter dataset. *International Journal of Remote Sensing*, 25, 3303-3330
- Stone, P.J., Sorensen, I.B., & Jamieson, P.D. (1999). Effect of soil temperature on phenology, canopy development, biomass and yield of maize in a cool-temperate climate. *Field Crops Research*, 63, 169-178
- Szigarski, C., Jagdhuber, T., Baur, M., Thiel, C., Parrens, M., Wigneron, J.-P., Piles, M., & Entekhabi, D. (2018). Analysis of the Radar Vegetation Index and Potential Improvements. In, *Remote Sensing*
- Tamhane, A.C. (2007). Multiple comparisons in model i one-way anova with unequal variances. *Communications in Statistics - Theory and Methods*, 6, 15-32
- Tedesco, D., de Oliveira, M.F., dos Santos, A.F., Silva, E.H.C., Rolim, G.D., & da Silva, R.P. (2021). Use of remote sensing to characterize the phenological development and to predict sweet potato yield in two growing seasons. *European Journal of Agronomy*, 129, 126337
- Tian, F., Cai, Z.Z., Jin, H.X., Hufkens, K., Scheifinger, H., Tagesson, T., Smets, B., Van Hoolst, R., Bonte, K., Ivits, E., Tong, X.Y., Ardö, J., & Eklundh, L. (2021). Calibrating vegetation phenology from Sentinel-2 using eddy covariance, PhenoCam, and PEP725 networks across Europe. *Remote Sensing of Environment*, 260, 112456
- Tran, K.H., Zhang, X., Ye, Y., Shen, Y., Gao, S., Liu, Y., & Richardson, A. (2023). HP-LSP: A reference of land surface phenology from fused Harmonized Landsat and Sentinel-2 with PhenoCam data. *Sci Data*, 10, 691
- Tukey, J.W. (1949). Comparing individual means in the analysis of variance. *Biometrics*, 5, 99-114
- van Hateren, T.C., Chini, M., Matgen, P., Pulvirenti, L., Pierdicca, N., & Teuling, A.J. (2023). On the potential of Sentinel-1 for sub-field scale soil moisture monitoring. *International Journal of Applied Earth Observation and Geoinformation*, 120, 103342
- Veloso, A., Mermoz, S., Bouvet, A., Le Toan, T., Planells, M., Dejoux, J.-F., & Ceschia, E. (2017). Understanding the temporal behavior of crops using Sentinel-1 and Sentinel-2-like data for agricultural applications. *Remote Sensing of Environment*, 199, 415-426

- Vijaywargiya, J., & Nidamanuri, R.R. (2023). Crop Phenology Extraction Using Big Geospatial Datacube, 1-4
- Villarroya-Carpio, A., Lopez-Sanchez, J.M., & Engdahl, M.E. (2022). Sentinel-1 interferometric coherence as a vegetation index for agriculture. *Remote Sensing of Environment*, 280, 113208
- Viña, A., Liu, W., Zhou, S., Huang, J., & Liu, J. (2016). Land surface phenology as an indicator of biodiversity patterns. *Ecological Indicators*, 64, 281-288
- Viswanathan, M., Scheidegger, A., Streck, T., Gayler, S., & Weber, T.K.D. (2022). Bayesian multi-level calibration of a process-based maize phenology model. *Ecological Modelling*, 474, 110154
- Wang, H.Q., Magagi, R., Goïta, K., Trudel, M., McNairn, H., & Powers, J. (2019). Crop phenology retrieval via polarimetric SAR decomposition and Random Forest algorithm. *Remote Sensing of Environment*, 231, 111234
- Wang, J., Song, G.Q., Liddell, M., Morellato, P., Lee, C.K.F., Yang, D.D., Alberton, B., Detto, M., Ma, X.L., Zhao, Y.Y., Yeung, H.C.H., Zhang, H.S., Ng, M., Nelson, B.W., Huete, A., & Wu, J. (2023). An ecologically-constrained deep learning model for tropical leaf phenology monitoring using PlanetScope satellites. *Remote Sensing of Environment*, 286, 113429
- Worrall, G., Judge, J., Boote, K., & Rangarajan, A. (2023). In-season crop phenology using remote sensing and model-guided machine learning. *Agronomy Journal*, 115, 1214-1236
- Xia, J., Niu, S., Ciais, P., Janssens, I.A., Chen, J., Ammann, C., Arain, A., Blanken, P.D., Cescatti, A., Bonal, D., Buchmann, N., Curtis, P.S., Chen, S., Dong, J., Flanagan, L.B., Frankenberg, C., Georgiadis, T., Gough, C.M., Hui, D., Kiely, G., Li, J., Lund, M., Magliulo, V., Marcolla, B., Merbold, L., Montagnani, L., Moors, E.J., Olesen, J.E., Piao, S., Raschi, A., Rouspard, O., Suyker, A.E., Urbaniak, M., Vaccari, F.P., Varlagin, A., Vesala, T., Wilkinson, M., Weng, E., Wohlfahrt, G., Yan, L., & Luo, Y. (2015). Joint control of terrestrial gross primary productivity by plant phenology and physiology. *Proc Natl Acad Sci U S A*, 112, 2788-2793
- Xin, Q.C., Li, J., Li, Z.M., Li, Y.M., & Zhou, X.W. (2020). Evaluations and comparisons of rule-based and machine-learning-based methods to retrieve satellite-based vegetation phenology using MODIS and USA National Phenology Network data. *International Journal of Applied Earth Observation and Geoinformation*, 93, 102189
- Yang, H.J., Pan, B., Li, N., Wang, W., Zhang, J., & Zhang, X.L. (2021). A systematic method for spatio-temporal phenology estimation of paddy rice using time series Sentinel-1 images. *Remote Sensing of Environment*, 259, 112394
- Yang, J.L., Dong, J.W., Liu, L., Zhao, M.M., Zhang, X.Y., Li, X.C., Dai, J.H., Wang, H.J., Wu, C.Y., You, N.S., Fang, S.B., Pang, Y., He, Y.L., Zhao, G.S., Xiao, X.M., & Ge, Q.S. (2023a). A robust and unified land surface phenology algorithm for diverse biomes and growth cycles in China by using harmonized Landsat and Sentinel-2 imagery. *ISPRS Journal of Photogrammetry and Remote Sensing*, 202, 610-636
- Yang, Z.J., Diao, C.Y., & Gao, F. (2023b). Towards Scalable Within-Season Crop Mapping With Phenology Normalization and Deep Learning. *IEEE Journal of Selected Topics in Applied Earth Observations and Remote Sensing*, 16, 1390-1402
- Yuan, H.H., Wang, X.Y., Jassal, R.S., Lu, L.L., Peng, J., & Wu, C.Y. (2022). Remote Sensing of Autumn Phenology by Including Surface Soil Temperature: Algorithm Development, Calibration, and Validation. *IEEE Journal of Selected Topics in Applied Earth Observations and Remote Sensing*, 15, 6485-6494
- Yuan, Y., Harer, S., Ottenheim, T., Misra, G., Lupke, A., Estrella, N., & Menzel, A. (2021). Maps, trends, and temperature sensitivities-phenological information from and for decreasing numbers of volunteer observers. *Int J Biometeorol*, 65, 1377-1390

- Zanaga, D., Van De Kerchove, R., De Keersmaecker, W., Souverijns, N., Brockmann, C., Quast, R., Wevers, J., Grosu, A., Paccini, A., Vergnaud, S., Cartus, O., Santoro, M., Fritz, S., Georgieva, I., Lesiv, M., Carter, S., Herold, M., Li, L., Tsendbazar, N.-E., Ramoino, F., & Arino, O. (2021). ESA WorldCover 10 m 2020 v100. In: Zenodo
- Zeng, L.L., Wardlow, B.D., Xiang, D.X., Hu, S., & Li, D.R. (2020). A review of vegetation phenological metrics extraction using time-series, multispectral satellite data. *Remote Sensing of Environment*, 237, 111511
- Zeyliger, A.M., Muzalevskiy, K.V., Zinchenko, E.V., & Ermolaeva, O.S. (2022). Field test of the surface soil moisture mapping using Sentinel-1 radar data. *Sci Total Environ*, 807, 151121
- Zhang, J., & Liu, Y. (2022). Decoupling of impact factors reveals the response of cash crops phenology to climate change and adaptive management practice. *Agricultural and Forest Meteorology*, 322, 109010
- Zhang, L.L., Zhang, Z., Luo, Y.C., Cao, J., Xie, R.Z., & Li, S.K. (2021). Integrating satellite-derived climatic and vegetation indices to predict smallholder maize yield using deep learning. *Agricultural and Forest Meteorology*, 311, 108666
- Zhao, W.Z., Qu, Y., Zhang, L.Q., & Li, K.Y. (2022). Spatial-aware SAR-optical time-series deep integration for crop phenology tracking. *Remote Sensing of Environment*, 276, 113046
- Zhou, J., Jia, L., Menenti, M., & Gorte, B. (2016). On the performance of remote sensing time series reconstruction methods – A spatial comparison. *Remote Sensing of Environment*, 187, 367-384
- Zhou, X., Xin, Q., Dai, Y., Li, W., & Qiao, H. (2021). A deep-learning-based experiment for benchmarking the performance of global terrestrial vegetation phenology models. *Global Ecology and Biogeography*, 30, 2178-2199